Master thesis and internship[BR]- Master's thesis : Conceptual Approach to Blown Wing Aircraft : Design and Performance Estimation - Based on Reverse Engineering Insights[BR]- Internship

Auteur : Dumont, Maxime
Promoteur(s) : Hillewaert, Koen
Faculté : Faculté des Sciences appliquées
Diplôme : Master en ingénieur civil en aérospatiale, à finalité spécialisée en "aerospace engineering"
Année académique : 2023-2024
URI/URL : http://hdl.handle.net/2268.2/20841

UNIVERSITÉ DE LIÈGE - FACULTÉ DES SCIENCES APPLIQUÉES

Conceptual Approach to Blown Wing Aircraft : Design and Performance Estimation

Based on Reverse Engineering Insights

Authors:

Maxime Dumont

Academic Supervisor:

Professor Koen Hillewaert

Company Supervisor:

Mr. Didier Breyne

Master's thesis carried out to obtain the degree of Master of Science in Aerospace Engineering by:
ACADEMIC YEAR 2023-2024

Abstract

This thesis explores the blown wing concept, focusing on propeller-driven systems and the development of a semi-empirical method for performance estimation. Based on Kuhn's approach, the method was integrated into the Aircraft Design Software (ADS) by OAD and enables quick and accurate estimations of lift, drag, and overall performance in the early stages of blown wing aircraft design.

Through detailed analysis, including the replication of 3D wind tunnel experiments using software, as well as comparisons with experimental data from the Breguet 941 and CFD simulations of the X-57 Maxwell, the method demonstrated robust performance in lift prediction, although refinements are needed for more precise longitudinal force estimation. The research also validated the method's application in assessing takeoff, landing, and minimum speed performance, confirming its utility in conceptual design phases.

Cette thèse explore le concept d'aile soufflée, en se concentrant sur les systèmes à hélices et le développement d'une méthode semi-empirique pour l'estimation des performances. Basée sur l'approche de Kuhn, la méthode a été intégrée dans le logiciel de conception d'avions (ADS) développé par OAD, permettant des estimations rapides et précises de la portance, de la traînée et des performances globales aux premières étapes de la conception d'avions à voilure soufflée.

À travers une analyse détaillée, incluant la reproduction d'expériences en soufflerie 3D à l'aide de logiciels, ainsi que des comparaisons avec les données expérimentales du Breguet 941 et les simulations CFD du X-57 Maxwell, la méthode a démontré une performance solide dans la prédiction de la portance, bien que des ajustements soient nécessaires pour une estimation plus précise de la force longitudinale. La recherche a également validé l'application de cette méthode pour évaluer les performances au décollage, à l'atterrissage et la vitesse minimale, confirmant son utilité dans les phases de conception conceptuelle.

Preface

This Master's thesis was conducted as part of an internship at Optimal Aircraft Design (OAD), based in Namur, Belgium. The methods and results developed herein are intended for use within the software developed by the company, ADS. ADS is an Aircraft Design Software used for reverse engineering, performance analysis, and various level of aircraft design.

Throughout the analysis, a significant number of methods from ADS were employed to estimate various parameters, such as the aircraft's drag coefficient, the lift characteristics of lifting surfaces, the efficiency of propellers and engines, among others. These methods, often semi-empirical and based on the geometry of the airplane, are primarily drawn from scientific sources and classical aircraft design literature, including works by Dr. Raymer, Dr. Roskam, and the USAF Stability and Control DATCOM.

While these methods are not the primary focus of this thesis and will not be elaborated upon in detail, certain critical techniques essential to understanding the overall approach will be introduced to clarify the limitations of the obtained results.

Additionally, the specific work done on the software code will not be disclosed due to the company's confidentiality requirements. Furthermore, this work is not directly relevant to the core findings of this study, despite constituting the majority of the effort undertaken during the internship.

Lastly, I would like to express my sincere gratitude to Mr. Breyne for giving me the opportunity to work at OAD. The completion of this work was made possible through his dedicated support and our daily exchanges, which also profoundly strengthened my passion and understanding of aircraft design.

Contents

List of Symbols

Table 0.0.1: List of Symbols

Symbol	Description
b	Span
c_f	Flap chord
c_w	Wing chord
C_D	Drag coefficient based on free-stream velocity, $C_D = \frac{D}{qS}$
C_L	Lift coefficient based on free-stream velocity, $C_L = \frac{L}{qS}$
$C_{L,off}$	Lift coefficient at power off
$C_{L,s}$	Lift coefficient based on slipstream velocity
C'_T	Thrust coefficient based on free-stream velocity, $C'_T = \frac{NT}{qS}$
$C_{T,s}$	Thrust coefficient based on slipstream velocity
C_X	Longitudinal-force coefficient based on free-stream velocity
$C_{X,s}$	Longitudinal-force coefficient based on slipstream velocity
D	Propeller diameter
D_{off}	Power-off wing drag
d	Diameter of fully developed propeller slipstream
e	Span efficiency factor
F	Resultant force
F_X	Longitudinal force
$\frac{F}{T}$	Thrust-recovery factor
i_w	Wing incidence
k	Empirical constant for correcting lift-augmentation term
L	Lift
L_{off}	Lift power off
$\dot{m}$	Mass flow
$\dot{m}_w$	Mass flow affected by the wing
$\dot{m}_s$	Mass flow affected by the propeller
N	Number of propellers
q	Free-stream dynamic pressure, $q = \frac{\rho}{2}V^2$
q_s	Slipstream dynamic pressure, $q_s = q + \frac{T}{S_p}$

Continued on next page

Table 0.0.1 – continued from previous page

Symbol	Description
S	Wing area
S_p	Propeller disk area
T	Thrust per propeller or total thrust when used in thrust recovery factor $\frac{F}{T}$
u	Increment of velocity due to thrust in fully developed slipstream
V	Free-stream velocity
V_{LO}	Lift-off velocity
V_A	Approach velocity
V_s or V_{min}	Stall or minimum velocity
ΔV	Vector change in velocity
w	Mass flow
α	Angle of attack
δ_f	Flap deflection
δ_e	Equivalent flap deflection due to wing camber
ϵ	Downwash angle due to wing lift
θ	Slipstream turning angle, measured from thrust axis
θ_w	Increment of turning angle due to wing camber
θ_f	Turning angle due to wing flap deflection
ρ	Air density

Chapter 1

Introduction

1.1 Motivation

Throughout the past and present centuries, a wide range of technologies and high-lift devices have been explored to improve the low-speed performance of aircraft without compromising their efficiency during cruise. The investigation into these technologies began as early as the 1920s, with the introduction of flaps, a concept that significantly increased lift during low-speed operations.

By the mid-20th century, further advancements were made with innovative methods such as externally or internally blowing high-speed airflow over the wing's surface to enhance lift and delay flow separation.

In the 1950s, both NASA, under the leadership of Richard E. Kuhn, and the Breguet company independently advanced these concepts by investigating the interaction between propeller slipstream and wing-flap systems. The central idea was to deflect the slipstream using the wing and flap, thereby increasing lift. NASA's research was primarily directed toward optimizing super Short Takeoff and Landing (SSTOL) and Vertical Takeoff and Landing (VTOL) operations, while Breguet focused on applying these principles to the design of a specific aircraft. Breguet's efforts culminated in the development of the Breguet 941, a military STOL transport aircraft equipped with large triple-slotted flaps placed directly in the slipstream of its four turboprop engines.

This concept, commonly referred to as the Externally Blown Wing or simply Blown Wing, has recently garnered renewed interest and is being actively revisited. Although it remains in use to some extent in modern military transport aircraft such as the Airbus A400M, Boeing C-17 Globemaster III, and the amphibious ShinMaywa US-2, its potential has been reignited by advancements in battery technology and the advent of electric motors in general aviation.

Electric motors, with their high power-to-weight ratios, compact straightforward installation, and excellent scalability, have enabled the development of highly distributed propulsion systems [1]. This concept, known as Distributed Electric Propulsion (DEP), allows for the entire wingspan to be equipped with distributed propellers, thereby enhancing the aerody-

namic interaction between the propeller, wing, and flap. As a result, innovative designs such as the NASA's X-57 Maxwell and Electra's eSTOL have emerged. The X-57, based on the Tecnam P2006T, utilizes 12 High Lift Propellers (HLP) exclusively during low-speed operations to maximize lift while maintaining a reduced wing surface area. The wing is thus highly optimized for cruise conditions and the HLPs are retracted during cruise. In turn, Electra's eSTOL demonstrator aircraft, equipped with eight propellers, has showcased exceptional STOL performance in flight tests.

In comparison to VTOL configurations— which have also seen renewed interest, particularly for air taxi applications— the blown wing configuration and STOL operations offer several distinct advantages during Take-off and Landing, including [2] :

- Reduced maximum power requirements
- Lower total energy consumption
- Reduced propulsion system weights

These factors are particularly critical for electric aircraft, which are constrained by the current limitations in energy-to-weight and power-to-weight ratios of batteries. Moreover, noise reduction is a significant consideration, especially for air taxis operating in close proximity to urban areas.

1.2 Main contributions of the present work

This research is centered exclusively on the blown wing concept utilizing propellers, although it acknowledges the existence of similar methods applicable to turbofans and turbojets.

The primary objectives of this work, based on reverse engineering of existing and conceptual aircraft (primarily the Breguet 941 and X-57), 3D wind tunnel experiments, and theoretical models, are as follows:

- To establish the design principles of a blown wing aircraft
- To assess the performance capabilities and limitations of blown wing aircraft
- To develop a semi-empirical method for rapid performance estimation. This method is designed to provide a quick and accurate approximation for various configurations, making it ideal for iterative processes during the conceptual design phase.

All the design principles, estimation methods, and identified limitations were developed with the objective of creating and implementing a performance analysis of distributed propulsion and blown wing systems within the company's software, ADS, developed by OAD. The implementation and coding of this analysis required significant time and effort, though the detailed process will not be discussed here. Furthermore, some specific methods from ADS,

based on scientific literature, were used in the estimations. While these methods won't be fully detailed, a few will be briefly introduced to provide context.

The structure of this thesis is organized as follows:

The second chapter offers a comprehensive overview of existing aircraft that utilize the blown wing concept, highlighting their most significant characteristics and performances. It also details the reverse engineering efforts conducted to understand their design and estimate their performance. This analysis sets the stage for the theoretical background explored in the following chapter.

The third chapter delves into the physical explanation of the blown wing phenomenon. The research then explores Kuhn's approach [3], discussing its foundational theory, methodology, and key parameters. This method serves as the core approach for all subsequent estimations conducted in this study. Its implementation within the Aircraft Design Software (ADS) is further elaborated, along with complementary estimation methods, their limitations, and potential areas for improvement. The limitations of the final developed method are then highlighted. Finally, static stability considerations specific to blown wing configurations are briefly discussed.

The fourth chapter focuses on the lift and drag characteristics of blown wing aircraft, serving two key purposes. First, it analyzes experimental data to understand the limits and potential of the blown wing concept. Second, it validates the effectiveness of the developed estimation method by comparing its results with the experimental data. To achieve this comparison, 3D wind tunnel experiments are replicated using ADS, allowing the derived values to be directly compared with the experimental data. Additionally, the lift and drag characteristics of the Breguet 941, as determined from flight data, and the X-57 Maxwell, as derived from CFD simulations, are thoroughly analyzed and compared against the estimated values.

The final chapter covers the performance of blown wing aircraft, focusing on takeoff, landing, and minimum speed. This analysis includes general considerations like safety margins and the impact of ground effect, which are important for understanding the operational limits of blown wing aircraft. The section also details the estimation methods developed in this research and compares the experimental and estimated performance of the Breguet 941, validating the proposed methods for use in conceptual design.

Chapter 2

Case studies and Reverse Engineering

2.1 Introduction

Various past and current aircraft incorporate the blown wing effect, such as the Breguet 941, ShinMaywa US-1/2 (seaplane), and to some extend, the C-17 Globemaster III and Airbus A400M [4]. Furthermore, innovative projects like NASA's X-57 Maxwell and Electra's eSTOL are currently in development. All of these aircraft are designed for STOL operations, exhibiting exceptional landing and takeoff performance.

A distinguishing feature of these designs is the use of flaps, typically slotted and extending across nearly the entire wingspan, positioned within the propeller slipstream. Another common characteristic is a large flap chord-to-propeller diameter ratio. This ratio is pivotal in efficiently deflecting the slipstream. The Breguet 941, for instance, utilizes large flaps to interact with the slipstream from its large turboprop engines. On the other hand, aircraft like NASA's X-57 and Electra's eSTOL use smaller, distributed electric propellers. These smaller propellers enable a high flap chord-to-propeller diameter ratio, even with high aspect ratio wings.

Throughout this dissertation, these configurations will serve as primary sources of information regarding the key design principles of blown wing aircraft. Consequently, some of them are briefly introduced and described herein.

Moreover, substantial data is available concerning the configurations and performance of the Breguet 941 and the X-57 Maxwell. Therefore, these aircraft will be reverse-engineered using ADS to achieve two primary objectives:

- To gain a comprehensive understanding of their design and performance procedures.
- To evaluate the accuracy and reliability of the methods developed in this study.

These two configurations, which serve as valuable sources of information, will be referenced throughout this work as key examples.

2.2 Breguet 941

Figure 2.2.1: Breguet 941 during approach with inboard/outboard flap deflected at 98°/65°, source unknown.

The Breguet 941 is a French, high wing, STOL aircraft designed in the 1960s. It was developed by Breguet Aviation with the primary objective of providing efficient and versatile transportation for both military and civilian purposes. The aircraft has a length of 73 feet and a wingspan of 78 feet, with a maximum takeoff weight of approximately 47,000 pounds. The four propellers are positioned so that the entire wing is within the slipstream. This configuration, coupled with the tripled slotted flap extending across the entire wingspan, significantly enhances the lift generated by the wing.

2.2.1 Description and replication

All the information used for the Breguet 941 was sourced from a flight investigation on the performance of the Breguet 941 conducted by NASA [5]. The aircraft's geometry was meticulously replicated in the Aircraft Design Software (ADS) based on the 3-view drawing presented in Fig.2.2.3 from the referenced document. Additionally, great care was taken to ensure that all surface areas, distances and characteristics listed in the accompanying table.2.2.2 were accurately respected. For more information, the reader is encouraged to refer to the NASA flight investigation.

Configuration	**Flap deflection (Inboard/Outboard)**
Landing configuration	98°/65°
Wave off	75°/50°
Take off	45°/30°

Table 2.2.1: Flap Deflection for various configurations

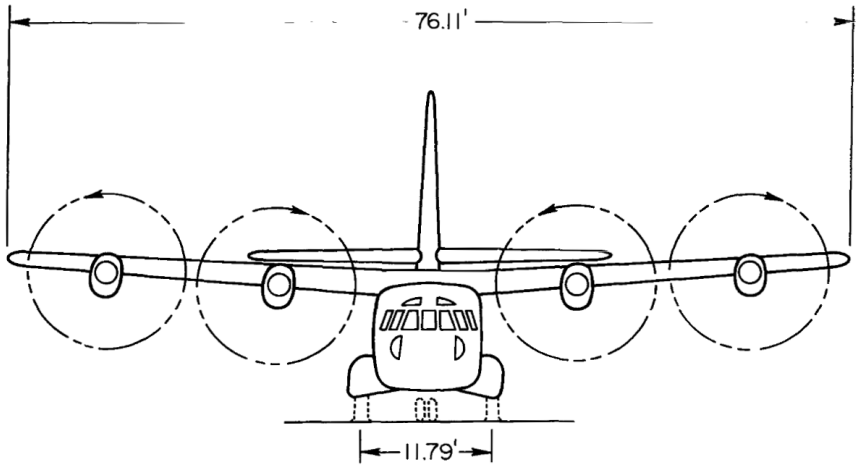

(a) Front view

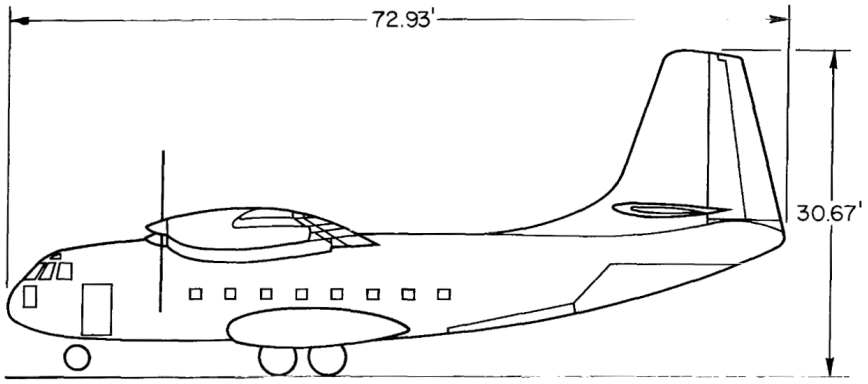

(b) Side view

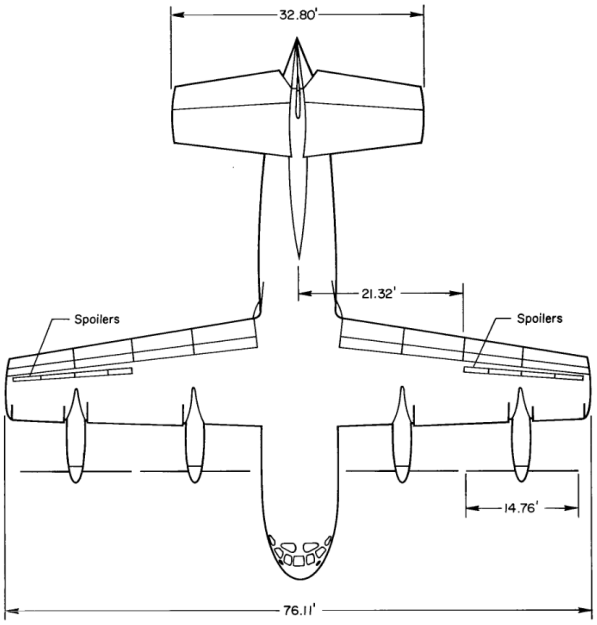

(c) Top view

Figure 2.2.2: 3 View drawing at scale.

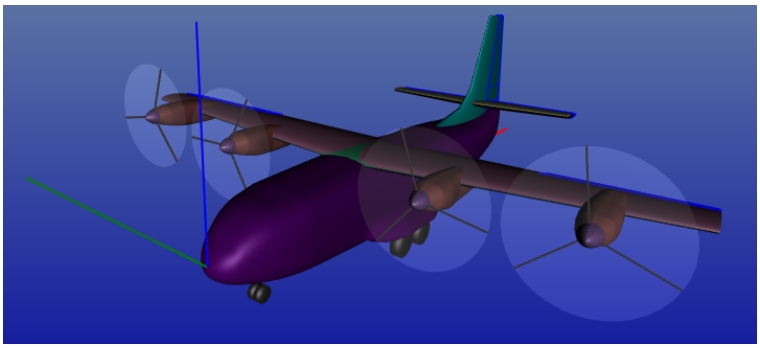

(a) Perspective

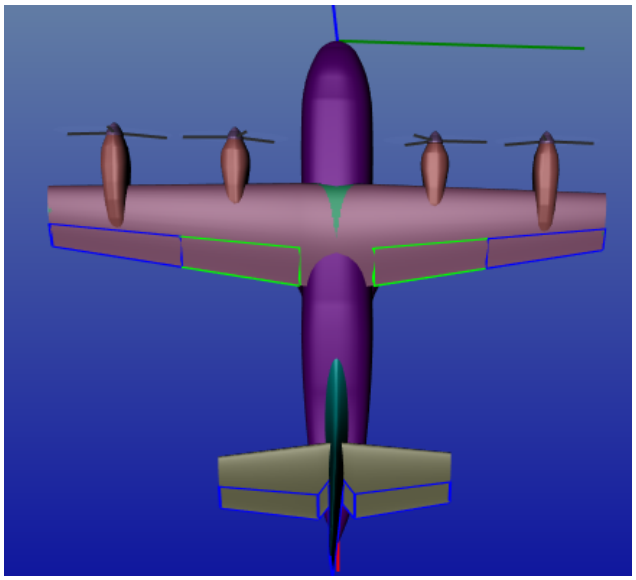

(b) Topview

Figure 2.2.3: View of the replicated Breguet 941 in ADS.

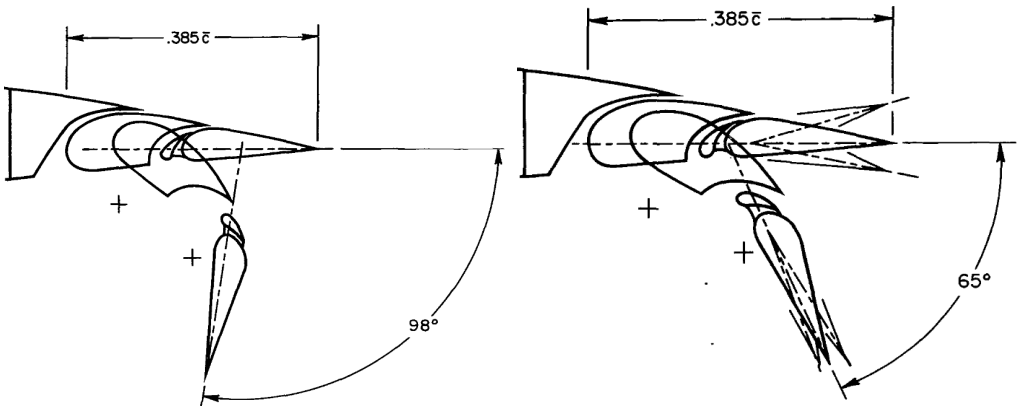

(a) Inboard triple slotted flap (b) Outboard triple slotted flap

Figure 2.2.4: Drawing at scale of the flaps in Landing configuration.

Table 2.2.2: Breguet 941 Data [5]

Wing	
Area	889 ft^2
Span	76.1 ft
Mean aerodynamic chord (reference)	12.15 ft
Incidence root, from fuselage reference line	3°
Twist	0°
Dihedral	4°
Airfoil section	63A416
Aspect ratio	6.52
Taper ratio	0.507
Type of flap	Triple slotted
Flap deflection (maximum)	98° internal, 65° external
Flap chord (c_f)	38.5% of wing chord
Spoiler spanwise location	From 56 to 97% of span
Spoiler deflection	45°
Spoiler chord, % chord	7
Horizontal Tail	
Total area	320 ft^2
Span	32.8 ft
Mean aerodynamic chord	9.92 ft
Airfoil section	63A212 inverted
Elevator area	119 ft^2
Elevator deflection	$-35°$ to $+25°$
Stabilizer deflection	$+1°$ to $+9°$ to fuselage ref.
Vertical Tail	
Total area	219 ft^2
Span	17.9 ft
Mean aerodynamic chord	13.1 ft
Airfoil section (modified)	63A013
Rudder area	82.6 ft^2
First rudder deflection	±20° first rudder
Second rudder deflection	±40° second rudder
Engine	
Number of propellers and engines	4
Type of engine	Gas turbine
Engine power	1165 hp
Propeller	
Type of propeller	Constant speed
Max Rotation speed	1200 RPM
Propeller diameter (D)	14.76 ft
Number of blade	3
Blade profile	Unknown
Distance from wing leading edge	0.38 D
Average $\frac{c_f}{D}$	0.31

2.2.2 Performance

A brief summary of the Breguet 941's performance is available in the table. These performance details will be further elaborated in the section related to the performance analysis of the Breguet 941.

Table 2.2.3: Aircraft Performance data obtained from experimental measurements at a weight of $38,500$ pounds

Performance	**Parameter**	**Value**
Take-off ($\delta_f = 45°/30°$)	Take-off speed	59 knots
	Ground roll on concrete	450 ft
	Total distance to 35 ft	900 ft
Landing ($\delta_f = 98°/65°$)	Approach speed	61 / 57 knots
	Ground roll on concrete	300 / 250 ft
	Total distance over 50 ft	650 / 850 ft
Cruise ($\delta_f = 0°/0°$)	Altitude	10000 ft
	True airspeed	225 knots
Minimum speed	Take-off configuration	44 knots ($C_{L_{max}} = 5$)
	Landing configuration	50 knots ($C_{L_{max}} = 6.7$)

2.2.3 Additional information regarding the Reverse engineering

The blade profile of the propeller is unknown, so a Hamilton Standard propeller was selected from the ADS database. This propeller was chosen due to its performance similarities with the thrust values provided at different power settings and phases of flight available in the NASA document (refer to Fig.29 of [5]). Comparing the performance of the selected propeller with that of the Breguet, a maximum difference of 3% in thrust was observed for flight speeds ranging from 45 to 110 knots. Additionally, it is indicated based on a 0.55 scale model in a wind tunnel that the propeller efficiency is 82% during cruise and that the static thrust was 4.2 pounds of thrust per shaft horsepower [5]. The selected blade had an efficiency of 85% under cruise conditions and produced 4.3 pounds of thrust per shaft horsepower in static conditions. This result indicates that the thrust may potentially be overestimated at very low speeds, such as during ground roll before lift off. The main characteristics of the selected blades are a design lift coefficient of 0.35 and an activity factor of 100.

2.3 NASA's X-57 Maxwell

Figure 2.3.1: Technical illustration of the X-57 Maxwell in flight, [NASA].

The NASA X-57 Maxwell is an electric experimental aircraft adapted from the Italian Tecnam P2006T, designed to showcase the benefits of distributed electric propulsion, including enhanced efficiency, reduced emissions, and lower operating costs. The X-57 features a significant modification from the traditional design, replacing conventional engines with two cruise wingtip propellers and 12 folding electric motors strategically mounted on redesigned, thinner wings.

The 12 electric motors are distributed along the wings to augment airflow and generate additional lift. This innovative propeller concept, known as the High Lift Propeller, is specifically designed to be used at low speeds. By operating exclusively during precise low-speed flight phases, the design of these propellers is streamlined, leading to improved performance and efficiency. This increased lift capability during takeoff and landing allows for a reduced wing surface area, thereby optimizing the aircraft for cruise conditions. The design of the X-57 was aimed at achieving the same performance as the Tecnam P2006T, but with reduced energy consumption and pollution. NASA's projections estimated a 50% reduction in the energy required for flight compared to the original configuration. Despite the project's cancellation at the end of 2023 due to budget overruns, the X-57 has contributed substantial data on design methodology, simulation analysis, and regulatory considerations. Simulations and analysis were conducted assuming a gross weight of 3,000 pounds.

2.3.1 Description and replication

Extensive documentation and technical papers related to the X-57 and its design procedure are freely accessible on NASA's X-57 technical paper page (https://www.nasa.gov/directorates/armd/x-57-technical-papers/). Some key design characteristics and all necessary information to simulate the aircraft in ADS was compiled from these sources. Specifically, the details provided

in Table.2.3.1 regarding the wing and flaps are sourced from [6]. Information concerning the propellers is derived from [7], and the CAD in Fig.2.3.2 is obtained from [8].

Table 2.3.1: X-57 Aircraft and High-Lift Propeller Design Parameters

Wing Characteristics	
Airfoil	GNEW5BP93B
Incidence	3.5°
Wing Area (S)	66.67 ft^2 (0.42 × original Tecnam)
Wing Loading (W/S)	45 lbs/ft^2
Aspect Ratio (AR)	15 (1.7 × original Tecnam)
Cruise C_L	0.75 (2.75 × original Tecnam)
Flap	
Type of flap	Single slotted
Flap chord	25% of wing chord
High-Lift Propeller Parameters	
Diameter (D)	1.88 ft
3/4 Pitch ($\beta_{3/4}$)	27.4°
Number of Blades	5
Speed	4549 RPM
Power (electric)	10.5 kW
Thrust	49.5 lbf
Flight Velocity	58 KTAS, Sea Level

2.3.2 Requirement and Performance

The aircraft requirements were as follows: a cruise speed of 150 knots at an altitude of 8,000 feet, a lift coefficient of 3.95 for a stall speed of 58 knots, and a cruise wing drag coefficient of 0.02191. According to calculations and simulations, the selected design meets these specifications.

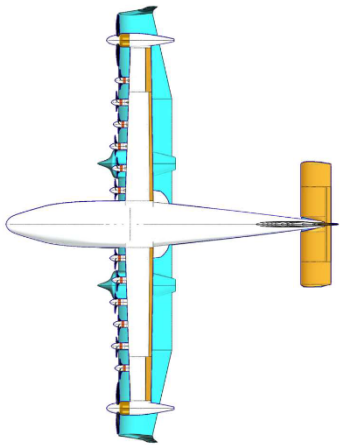

(a) A Comparative Analysis of the X-57 Wing and the Tecnam P2006T:

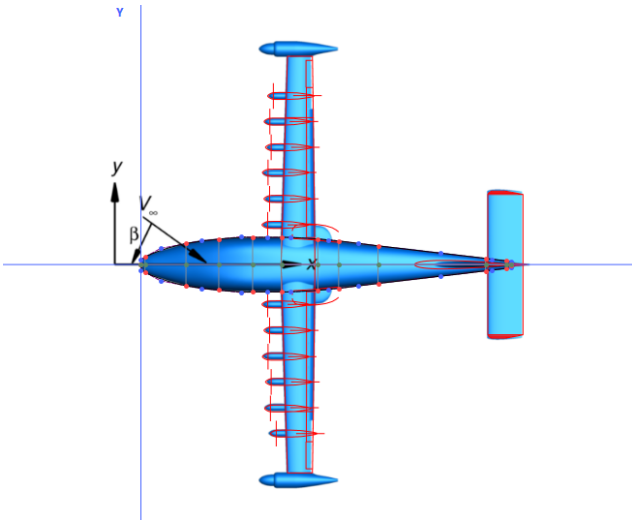

(b) Top view superposition of the X-57 and its replication in ADS

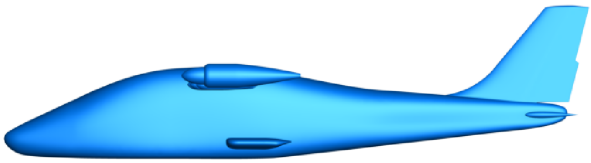

(c) Lateral view of the X-57

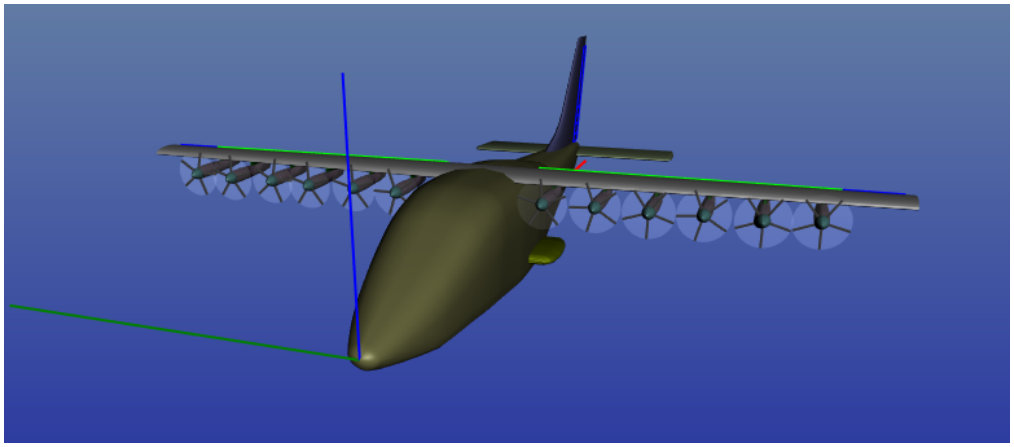

(d) X-57 replicated without its Cruise propellers

Figure 2.3.2: Various views of the Tecnam P2006T, X-57 and its replication.

2.4 Shinmaywa US-2

Figure 2.4.1: Shinmaywa US-2 during take-off from water [https://www.shinmaywa.co.jp/].

The ShinMaywa US-2 is a Japanese amphibious aircraft designed for search and rescue operations, featuring advanced STOL capabilities. Developed by ShinMaywa Industries, the US-2 is an evolution of the earlier US-1A model, incorporating modern technologies to enhance performance and operational range. The aircraft is equipped with four turboprop engines, and its high-wing configuration and large flaps significantly contribute to its exceptional STOL performance (see Fig.2.4.2).

Moreover, the US-2 employs a specific engine system to internally blow air over the plain flap, tail and control surfaces, a technique known as boundary layer control (BLC). This system delays the onset of stall by maintaining smoother airflow over the wings at lower speeds, thereby significantly enhancing lift. The BLC system works by channeling high-pressure air from the engines through ducts to small jets located along the leading edges and control surfaces of the wings (see Fig.2.4.3).

There is insufficient information available to fully replicate the aircraft, and its boundary layer control system cannot be accurately modeled in ADS. Nevertheless, it serves as a valuable source of information within the context of this study, offering insights that are pertinent to the objectives and analyses conducted.

2.4.1 Description and performance

The geometric and performance data for the aircraft have been sourced from *Jane's All the World's Aircraft 2007-2008* [9].

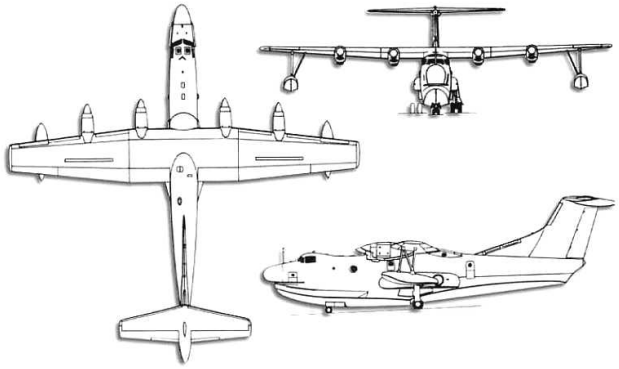

Figure 2.4.2: 3-view on ShinMaywa US-1/2 from [9]

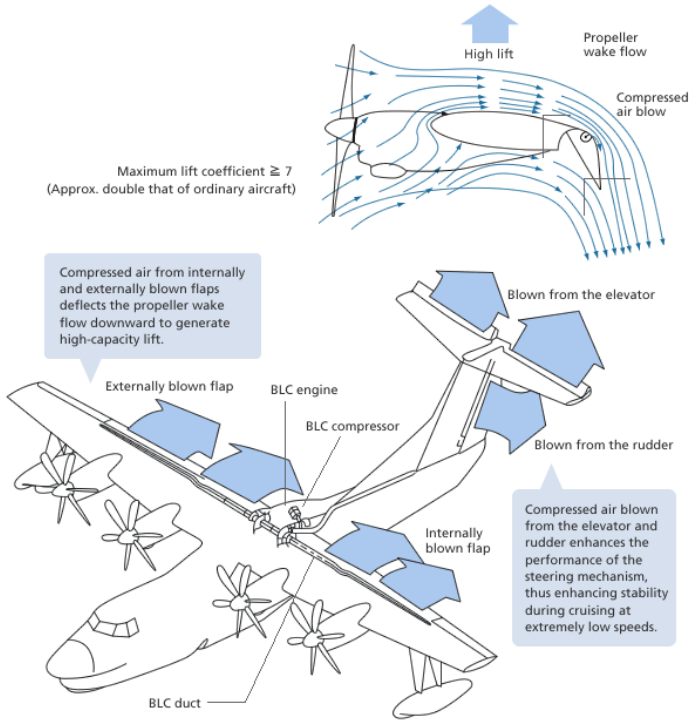

Figure 2.4.3: Boundary layer control and blown flap technology, [extracted from : https://www.shinmaywa.co.jp/].

Table 2.4.1: Aircraft Dimensions.

Parameter	**Value**
Wing span	108 ft
Length overall	109 ft
Height overall	32 ft
Tailplane span	40 ft
Wing and Areas	
Wing chord at root	16 ft
Wing chord at tip	7 ft
Wing aspect ratio	8.1
Wings, gross	$1,462.0$ ft^2
Inner flaps (total)	101.3 ft^2
Outer flaps (total)	152.85 ft^2
Fin	189.0 ft^2
Rudder	75.0 ft^2
Tailplane	248.0 ft^2
Engine/propeller Turboprop engine power	$4,591$ shp each
BLC Engine power	$1361,137$ hp
Propeller diameter	14 ft
Number of blades	6
Weights and Loadings	
Manufacturer's weight empty	$51,367$ lb
Max T-O and landing weight (land, US-2)	$105,160$ lb
Max wing loading	67.85 lb/ft^2

Table 2.4.2: Aircraft Performance at 79,365 lb, sea level.

Condition	**Details**	**Distance**
T-O distance on water	40° flap, BLC on	$1,820$ ft
Landing on land	60° flap, BLC on, with reverse pitch	$2,655$ ft
Landing on water	60° flap, BLC on	720 ft

Chapter 3

Theoretical Background

3.1 Propeller-Wing-Flap Interaction

The interaction between the propeller slipstream and the wing has been the subject of extensive research, with numerous studies documented in the literature. While the blown wing concept will be further elaborated using momentum theory in the section dedicated to Kuhn's approach, this section provides a concise overview of the critical aspects of the Propeller-Wing-Flap interaction. The insights presented here are based from experimental data. For a more in-depth information, readers are encouraged to consult the PhD theses of M. D. Patterson [10], and L. Veldhuis [11].

3.1.1 Key Performance Enhancements Due to Propeller-Wing-Flap Interaction

1. **Increased Lift via Slipstream Deflection:** The high-speed slipstream generated by the propeller, when deflected by the wing and flaps, significantly increases lift. This phenomenon occurs due to the change in the vertical momentum of the slipstream, which results in an additional upward lift force acting on the wing [10].

2. **Delayed Flow Separation and Wake Bursting:** At high angles of attack or with substantial flap deflection, the propeller slipstream plays a crucial role in delaying flow separation and preventing wake bursting. This is primarily achieved by the introduction of the propeller slipstream's high total pressure over the wing and through the flap gap, thereby energizing the boundary layer [12].

   It has also been observed that the slipstream causes the boundary layer to transition between laminar and turbulent states at a frequency corresponding to the propeller blade passage [13]. Furthermore, increasing the number of propeller blades amplifies this effect by raising the frequency of blade passage, which in turn increases turbulence intensity. Some studies even suggest that this increase can lead to the complete elimination of the cyclic transition, resulting in a fully turbulent boundary layer over the

wing [14]. Although a fully turbulent boundary layer increases friction drag, it also improves flow attachment, allowing the wing to maintain lift at higher angles of attack and flap deflections.

Additional experimental studies, such as those by Catalano [15], have shown that the laminar separation bubble that occur at power off, can effectively be eliminated when within the slipstream. This research also indicates that the influence of the slipstream extends beyond the immediate propeller radius due to viscous mixing with the external flow. Further research by Aminaei et al. [16][17] supported this conclusion, demonstrating that the slipstream not only promoted the transition of the boundary layer but also shifted its onset closer to the leading edge. Moreover, increases in propeller rotational speed and thrust caused the turbulent flow to envelop the entire wing surface, washing out the laminar separation bubble.

Finally, at low speeds and high thrust angle, the inclined propeller can partially reorient the flow along the wing chord direction, further delaying stall compared to a "power-off" wing configuration [18].

The overall effect of these interactions results in better performance of highly deflected flaps and a significant improvement in the wing's stall characteristics. Wind tunnel results discussed in Chapter 4, along with the lift and drag characteristics of the Breguet 941 and X-57, support this observation. At very high power settings, the Breguet 941 does not exhibit a typical stall; even with inboard flaps deflected at 98°, the aircraft experiences only a slight reduction in lift beyond the maximum lift coefficient (Cl_{max}), resulting in relatively flat lift curves above this threshold. Similarly, CFD simulations of the X-57 reveal comparable behavior.

In addition to the effects mentioned above, the propeller also induces a swirl in the slipstream, which alters the angle of attack along different sections of the wing. Specifically, the sections of the wing positioned behind the upward-moving half of the propeller plane encounter an increase in angle of attack, while those aft of the downward-moving half experience a decrease [10]. This effect significantly modifies the lift distribution across the wing. This phenomenon, which is not studied in this paper, seems to be particularly significant for the design of the X-57, which features 12 high lift propellers with high design lift coefficient [10] [19] [20].

3.2 Kuhn's Approach : Momentum theory and Estimation procedure

In this section, the methodologies employed to calculate the aerodynamic forces of a blown wing throughout this work are detailed. This approach is largely based on the semi-empirical method developed by Kuhn in the 1950s, which relies on momentum theory.

Therefore, the first part of this section is devoted to an in-depth explanation of Kuhn's approach. This includes a discussion of the theoretical foundations of his procedure, which also provides a physical explanation for the blown wing effect. Following this theoretical overview, the lift and drag equations are highlighted, with particular emphasis on the key parameters that are crucial for assessing blown wing performance.

All theoretical developments, equations, and graphs in this part are extracted from the NASA's memorandum by Kuhn [3], and this portion of the section serves merely as a summary. Readers are strongly encouraged to consult the original document for more complete information.

Subsequently, the focus shifts to the implementation of Kuhn's method within the Aircraft Design Software (ADS), detailing any modifications made and the integration of supplementary estimation techniques. These complementary methods, primarily drawn from Roskam's Aircraft Design [21], are used to determine the "power off" aerodynamic characteristics of the wing.

The section concludes with an analysis of the limitations inherent in the procedure, as well as the specific conditions under which it is most applicable.

3.2.1 Basis of analysis

Aircraft generate lift by deflecting air downward with their wings. As assumed in the momentum theory, the air mass flow deflected by the wing is contained within a stream tube, which has the wing's span as its diameter.

Thrust, on the other hand, is produced by accelerating air rearward through the action of the propeller. The resulting slipstream, which is the stream tube of air accelerated by the propeller, can also be deflected downward. This deflection can be achieved either by tilting the thrust axis or by the wing-flap configuration. When the slipstream is deflected downward, a portion of the thrust is converted into additional lift.

In the context of a propeller-wing system, as shown in Fig.3.2.1, the airflow can be conceptualized as consisting of two distinct stream-tube systems:

1. **The Wing-Affected Stream Tube:** This larger stream tube represents the mass flow influenced by the wing, which is deflected by a small average angle, denoted as ϵ.
2. **The Propeller Slipstream:** The smaller stream tubes represent the mass flow accel-

erated by the propeller, known as the slipstreams. These slipstreams can be deflected through a larger angle, denoted as θ, depending on the configuration of the wing and flaps.

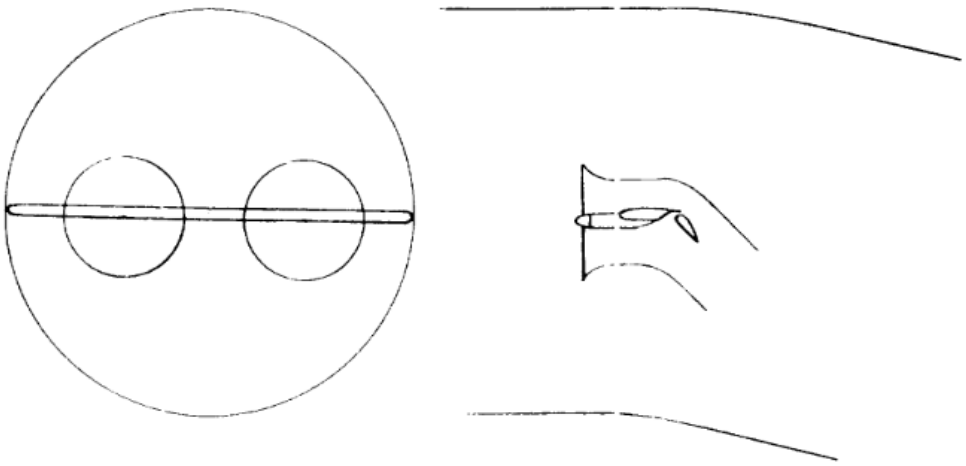

Figure 3.2.1: Sketch representing the various mass flows considered in the momentum theory method [3].

In Kuhn's approach, the forces generated by the acceleration and deflection of each of these stream tubes are analyzed separately. The slipstream deflection is estimated based on experimental slipstream data at zero forward speed while the force on the wing due to the large stream tube is based on the conventional power-off wing-flap information.

The lift and drag contributions from both the wing and the propeller slipstreams are then combined to provide a comprehensive method for estimating the overall aerodynamic performance of a blown wing.

Power-off wing characteristics

The mass flow of air, $\dot{m}_w$, within the stream tube affected by the wing can be expressed as:

$$\dot{m}_w = \frac{\pi}{4} b^2 \rho V \tag{3.2.1}$$

This stream tube, influenced by the wing, is deflected by an angle ϵ, resulting in a velocity change in the direction of lift:

$$\Delta V = V \sin \epsilon \tag{3.2.2}$$

Consequently, the lift force generated by the wing can be formulated as:

$$L = \frac{\pi}{4} b^2 \rho V^2 \sin\epsilon \tag{3.2.3}$$

During this process of deflecting the stream tube downward, there is also a resultant velocity change in the drag direction, which can be described by:

$$\Delta V = V - V\cos\epsilon \tag{3.2.4}$$

Therefore, the drag associated with the generation of lift is given by:

$$D = \frac{\pi}{4} b^2 \rho V^2 (1 - \cos\epsilon) \tag{3.2.5}$$

By solving for V in equation 3.2.3 and substituting the result into equation 3.2.5, and then applying the small-angle approximation, we can simplify the expression to yield the well-known relation for induced drag:

$$C_{D,i} = \frac{C_L^2}{\pi AR} \tag{3.2.6}$$

With AR, the aspect ratio.

Propeller slipstream characteristics

As shown in Fig.3.2.7, at zero forward speed, deflecting the thrust generates lift. In Kuhn's approach, the forces generated by the thrust are generally presented in terms of the turning angle θ and thrust recovery factor $\frac{F}{T}$. θ is defined as the deflection of the slipstream and highly depends on the flap deflection. The thrust recovery factor (TRF), is the ratio of thrust that actually generates force on the wing. As will be shown later, the TRF is generally close to 1 but some part of the thrust can be lost due to non-uniform flow or high deflection of the flap.

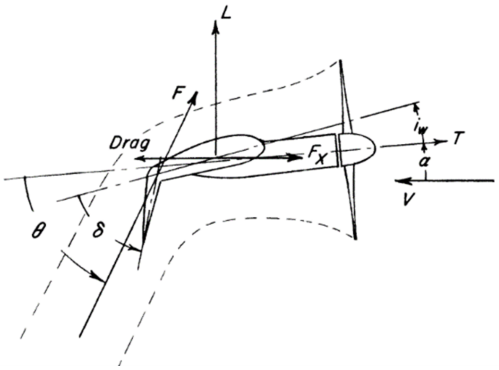

Figure 3.2.2: Sketch representing the slipstream behind the propeller under static thrust conditions.[3]

The lift can then be defined as :

$$L = \frac{F}{T} NT \sin(\theta + \alpha) \tag{3.2.7}$$

With N being the number of propellers, F,the resultant force of the thrust applied on the aircraft, T, the thrust and α, the angle of attack

And the longitudinal force as :

$$F_X = \frac{F}{T} NT \cos(\theta + \alpha) \tag{3.2.8}$$

At forward speed, however, this effect is not the only one contributing to lift. As previously stated, thrust is generated by accelerating the slipstream air. The increase in speed results in a higher total mass flow, $\dot{m}$, compared to the unpowered configuration. This additional mass of air is deflected by the wing, thereby resulting in increased lift.

Using momentum theory applied to propeller and assuming fully developed slipstream at the propeller disk, one can find :

The mass flow of air in the slipstream :

$$\dot{m}_s = \frac{\pi}{4} D^2 \rho \left(V + \frac{u}{2} \right) \tag{3.2.9}$$

And the thrust :

$$T = \dot{m}_s u = \frac{\pi}{4} D^2 \rho \left(V + \frac{u}{2} \right) u \tag{3.2.10}$$

With u the increment of velocity attained in the fully developed slipstream.

Lift and Drag equations based on wing and slipstream mass flow

Now that that both mass flow are defined, we can define the total mass flow of the system as :

$$\dot{m} = N\dot{m}_s + \dot{m}_w - \dot{m}_c = N\frac{\pi}{4} D^2 \rho \left(V + \frac{u}{2} \right) + \frac{\pi}{4} b^2 \rho V - N\frac{\pi}{4} D^2 \rho V \tag{3.2.11}$$

The first term is the mass flow within the N propeller slipstreams, the second is the main mass flow affected by the wing. The third term $\dot{m}_c$ is a correction for the fact that the slipstreams occupy space within the win stream tube. It is also presumed that the fully contracted slipstream is obtained at the wing and that it does not modify the diameter of the overall stream tube.

Now by adding the appropriate downward increment velocity on each term and assuming theta does not change with the free stream velocity, the lift equation is obtained :

$$L = \frac{F}{T} N \frac{\pi}{4} D^2 \rho \left(V + \frac{u}{2}\right) (V + u) \sin(\theta + \alpha) + \frac{\pi}{4} b^2 \rho V^2 \sin\epsilon - \frac{F}{T} N \frac{\pi}{4} d^2 \rho V^2 \sin(\theta + \alpha) \quad (3.2.12)$$

Noting that,

$$T = \frac{\pi}{4} D^2 \rho \left(V + \frac{u}{2}\right) u \quad (3.2.13)$$

The lift can be written as :

$$L = L_{off} + \frac{F}{T} NT \sin(\theta + \alpha) + \frac{F}{T} N \frac{\pi}{4} D^2 \rho V^2 \sin(\theta + \alpha) \left(1 + \frac{u}{2V} - \frac{d^2}{D^2}\right) \quad (3.2.14)$$

Reducing to coefficient form it gives :

$$C_L = C_{L,off} + \frac{F}{T} C'_T \sin(\theta + \alpha) + \frac{F}{T} C'_T \sin(\theta + \alpha) \frac{1}{\sqrt{1 + \frac{C'_T S}{N S_p}}} \quad (3.2.15)$$

Similarly, the longitudinal force can be computed as :

$$F_X = \frac{F}{T} NT \cos(\theta + \alpha) - D_{off} - \frac{F}{T} N \frac{\pi}{4} D^2 \rho V^2 \left[1 - \cos(\theta + \alpha)\right] \frac{1}{\sqrt{1 + C'_T \frac{S}{N S_P}}} \quad (3.2.16)$$

And reduced to ciefficient form,

$$C_X = \frac{F}{T} C'_T \cos(\theta + \alpha) - C_{D,off} - \frac{F}{T} C'_T \left[1 - \cos(\theta + \alpha)\right] \frac{1}{\sqrt{1 + C'_T \frac{S}{N S_P}}} \quad (3.2.17)$$

3.2.2 Methodology: Estimation of Lift and Longitudinal Force Coefficients

The lift and longitudinal force equations presented here correspond to the final equations 3.2.15 and 3.3.1 in the theoretical development of Kuhn's approach, with one notable exception. These equations have been adjusted by Kuhn through the introduction of a correction factor '$k = 1.8$' in the third term to better align with experimental data. Kuhn primarily attributes the discrepancy between the original estimation equation and the experimental results to the simplifying assumption that the angles θ and ϵ are constant and independent of each other, which does not fully capture the complexities of the actual flow dynamics. In reality, the turning angle is likely reduced due to the influence of the main stream tube, while the downwash angle may be increased as a result of the slipstream interaction.

$$C_L = C_{L,off} + \frac{F}{T} C'_T \sin(\theta + \alpha) + k \frac{F}{T} C'_T \sin(\theta + \alpha) \frac{1}{\sqrt{1 + \frac{C'_T S}{N S_p}}}$$

$$= C_{L,off} + C_{L,2} + C_{L,3}$$

With :

- $C_{L,off}$, the power-off lift coefficient
- $\frac{F}{T}$, the thrust recovery factor
- N, the number of propellers
- T, the thrust of one propeller
- $C'_T = \frac{NT}{qS}$, the total thrust coefficient
- θ, the turning angle
- α, the angle of attack
- S, the wing surface
- S_p, the propeller disk area

As illustrated in Fig.3.2.3, the first term corresponds to the lift coefficient of the wing in a power-off condition, representing the baseline aerodynamic lift. The second term accounts for the direct contribution of thrust to the overall lift, reflecting the force generated by the propulsion system. Lastly, the final term captures the effect of increased mass flow within the system due to the elevated velocity in the propeller slipstream, further contributing to the overall lift generated by the aircraft.

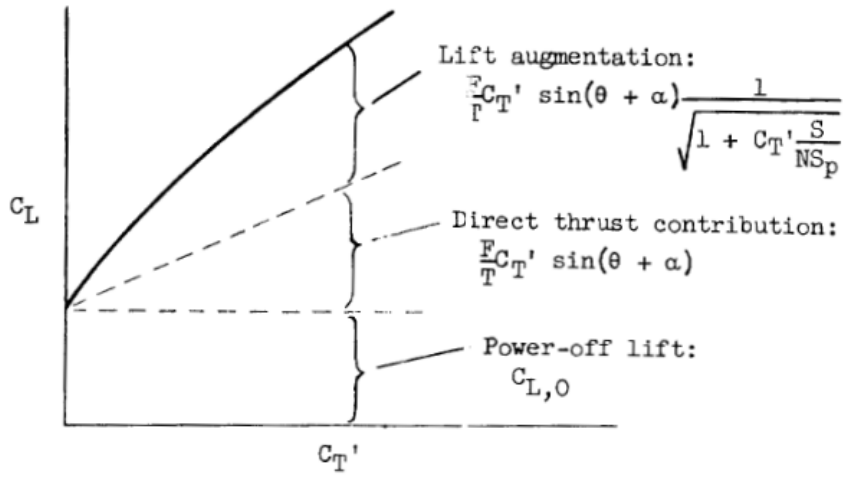

Figure 3.2.3: Sketch representing the various contributions to lift with respect to the thrust coefficient [3].

Similarly, the longitudinal force coefficient can be computed as :

$$C_X = \frac{F}{T} C_T' \cos(\theta + \alpha) - C_{D,off} - k \frac{F}{T} C_T' \left[1 - \cos(\theta + \alpha)\right] \frac{1}{\sqrt{1 + C_T' \frac{S}{NS_P}}} \tag{3.2.18}$$

All the terms contributing to the longitudinal force with respect to the thrust coefficient are showned in Fig3.2.4

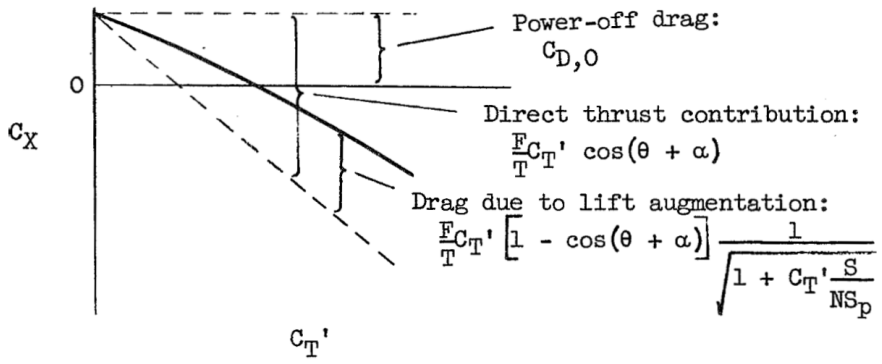

Figure 3.2.4: Sketch representing the various contributions to longitudinal force with respect to the thrust coefficient [3].

Each parameter within these equations is crucial to the enhanced lift characteristics observed in blown wing configurations. Consequently, a comprehensive analysis of these key parameters will be conducted, with a focus on the methods used to estimate them. These methods, developed by Kuhn, are based on experimental data.

3.2.3 Key Parameters for blown wing performance

Power-off Lift and Drag

The propeller slipstream has the potential to eliminate stalling at high power settings. As a result, wings that would stall under power-off conditions often remain unstalled when operating with a moderate to high propeller thrust coefficient. Therefore, when analyzing lift and drag, it is crucial to consider the values that would be attained if the wing were in an unstalled state under power-off conditions. The method used in this analysis does not predict stall behavior, and it is essential to apply it only within the unstalled flight regime to ensure the accuracy and validity of the results. With this consideration in mind, the lift coefficient should be estimated using the following equation:

$$C_L = C_{L_\alpha} \sin(\alpha - \alpha_0) \tag{3.2.19}$$

With C_{L_α} and α_0 being respectively the lift slop and the zero lift angle in radian.

Thrust Recovery Factor

The Thrust Recovery Factor (TRF) represents the proportion of the accelerated airflow, or thrust, that is effectively deflected by the wing flaps. Any thrust not deflected by the flaps is considered lost and neither contributes to the aircraft's thrust nor to its lift. The TRF is primarily influenced by the number of propellers per wing span, the turning angle, and the nacelle. Inadequate integration between the nacelle and the wing can lead to substantial reductions in thrust recovery [22]. Furthermore, at high angles of attack, nacelles can significantly disrupt the airflow, leading to a decrease in wing performance. Even in the X-57 design, which features small, meticulously designed nacelles for its compact electric motors, there is an estimated reduction of 0.25 in the lift coefficient when the angle of attack exceeds 10 degrees [23].

The TRF is determined from experimental data, presented in Fig3.2.5, which is derived from wind tunnel tests involving wings equipped with nacelles. This means that the influence of nacelles is indirectly accounted for in the method. However, the method does not take into consideration the specific size, profile, or number of nacelles as input parameters, meaning their effect is assumed constant across different configurations. Furthermore, it is important to note that the experimental data does not cover configurations with more than two propellers per semispan. Thus, the thrust recovery factor has been adjusted for large distributed propulsion configurations, where the previous condition of "two propellers per semi-span" is considered analogous to a large-span flap fully immersed in the slipstream. In cases where less than 50% of the wing and flap are exposed to the slipstream, the configuration is treated similarly to the former "one propeller per semi-span" condition. For configurations that fall between these two extremes, interpolation is applied to determine the thrust recovery factor. This adjustment is unlikely to introduce significant error, as the TRF is generally close to one and is not expected to be reduced in modern DEP configurations.

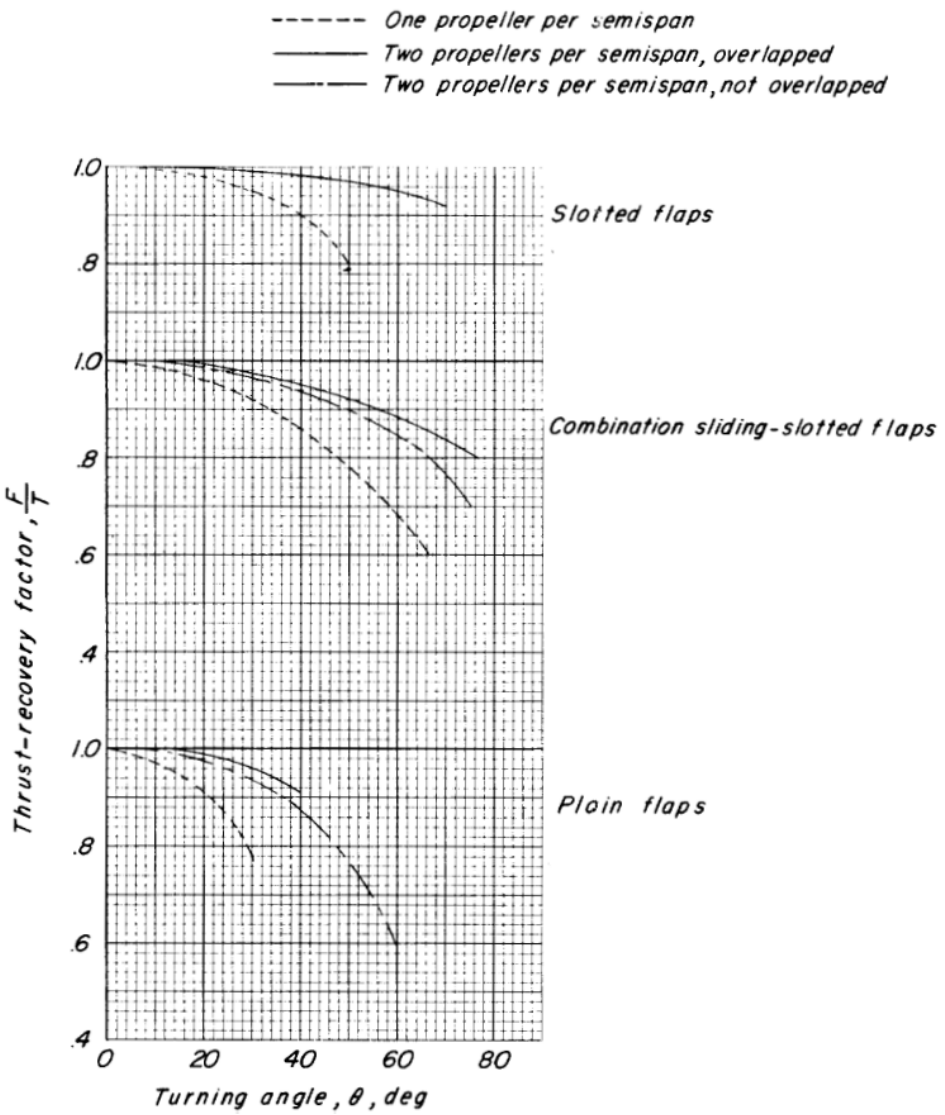

Figure 3.2.5: Thrust recovery factor with respect to the turning angle for various configurations

Turning Angle and Flap Chord-to-Wing Ratio

The turning angle θ is a parameter that quantifies the deflection of the propeller slipstream as it interacts with the wing and flap system. This variable is crucial as it directly influences the conversion of thrust into lift.

This angle is influenced by several factors, including the type of flap being utilized, the flap deflection angle (δ), and the ratio of the extended flap chord to the propeller diameter ($\frac{c_f}{D}$). Accurate estimation of the turning angle is essential for predicting the aerodynamic behavior of blown wing configurations.

The turning angle estimation is derived from empirical data, as depicted in Fig. 3.2.6. This figure presents the relationship between the turning angle and the flap deflection, pa-

rameterized by the ratio $\frac{c_f}{D}$. It is important to note that the values provided in Fig. 3.2.6 have been adjusted to exclude the effects of wing camber, ensuring that the turning angle reflects only the influence of flap deflection and propeller slipstream interaction.

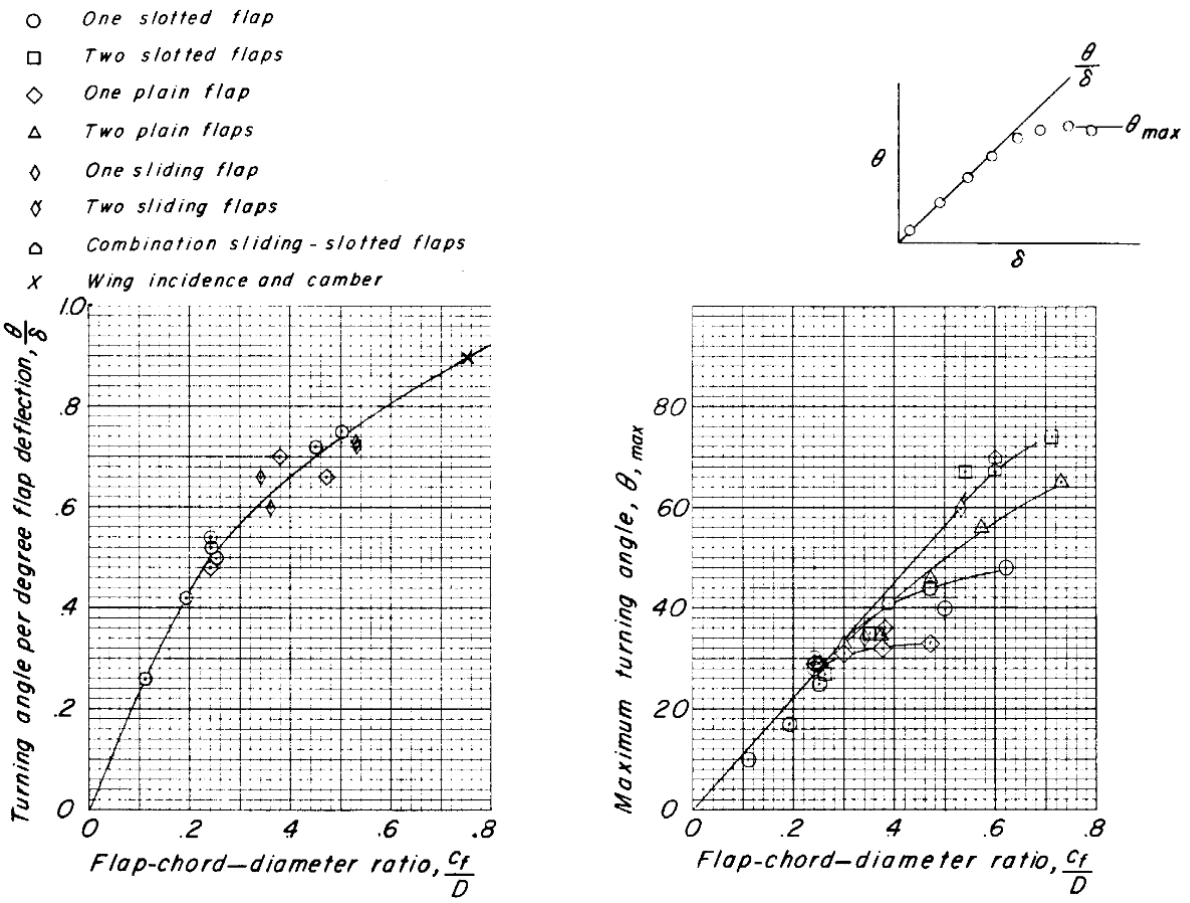

Figure 3.2.6: Ratio of Turning Angle to Flap Deflection and Maximum Turning Angle with Respect to $\frac{c_f}{D}$

Once the ratio known, the turning angle due to the flap is computed as :

$$\theta_f = (\frac{\theta}{\delta})_f \times \delta \tag{3.2.20}$$

In addition of the turning angle due to the flaps, the turning angle due to the camber of the wing needs to be added. This increment in turning angle can be estimated, for low cambered airfoil, by defining a equivalent deflection δ_e and following the same procedure. δ_e is defined by the angle between the thrust axis and the mean camber line at the trailing edge.

This increment in turning angle $\Delta\theta$ is then computed using the ratio of the wing chord over the propeller diameter $\frac{c_w}{D}$ instead of $\frac{c_f}{D}$:

$$\theta_w = (\frac{\theta}{\delta})_w \times \delta_e \tag{3.2.21}$$

It is then possible to compute the total turning angle by adding the two terms :

$$\theta = \theta_f + \Delta\theta \tag{3.2.22}$$

As shown in Fig3.2.6, the maximum turning angle, which directly governs the maximum lift coefficient achievable for a given thrust, is also critically influenced by the ratio of the extended flap chord to the propeller diameter (c_f/D) and the specific type of flap used. The maximum turning angle essentially represents the limit beyond which the linear relationship between flap deflection and turning angle no longer holds, as further deflection leads to flow separation and flap stall.

Therefore, for a given level of thrust, the c_f/D ratio stands out as a pivotal parameter in determining the aerodynamic performance of a blown wing aircraft. When propellers are large in diameter, it becomes imperative that the flaps are sufficiently large to achieve the necessary deflection to fully leverage the propeller slipstream. This requirement can have a profound impact on the overall design of the wing, often necessitating a larger wing chord to maintain this ratio.

A prime example of this is the Breguet 941, which utilizes four turboprops, each with a diameter of 14.7 feet, to achieve both blown wing effects and efficient cruise performance. To fully exploit the potential of these propeller slipstreams at low speeds, the aircraft employs a wing with a relatively low aspect ratio of 6.5 and triple-slotted flaps with a chord length of 1.8 meters.

The advent of Distributed Electric Propulsion (DEP) technology has introduced new possibilities for wing and propeller design configurations. With smaller propeller diameters now being feasible, it is possible to design wings with higher aspect ratios while still achieving a favorable c_f/D ratio. This configuration allows for the full exploitation of the blown wing effect, without the need for excessively large wing chords. NASA's X-57 concept illustrates this approach, utilizing smaller diameter propellers to maintain aerodynamic efficiency while capitalizing on the benefits of the blown wing effect.

3.3 Implementation of Kuhn's Method and complementary estimation techniques

3.3.1 Final Version of the Method

The Kuhn method, including its empirical estimations for the Thrust Recovery Factor ($\frac{F}{T}$), turning angle, and maximum turning angle, has been adapted and integrated into the Aircraft Design Software (ADS).

To enhance the precision of these estimations, the turning angle and TRF are computed individually for each propeller, taking into account the specific characteristics of the wing-flap section located downstream. This refined approach allows for the accommodation of varying flap types, sizes, and propeller diameters within a single design framework. Consequently, the equations governing drag and lift coefficients, while fundamentally similar to the original formulations, have been adjusted to reflect these variables :

$$\begin{aligned} C_L &= C_{L,off} + \sum_{n=1}^{N} \frac{F}{T} C_T'' \sin(\theta_n + \alpha_n) + \sum_{n=1}^{N} k \frac{F}{T} C_T'' \sin(\theta_n + \alpha_n) \frac{1}{\sqrt{1 + \frac{C_T'' S}{S_p}}} \\ &= C_{L,off} + C_{L,2} + C_{L,3} \end{aligned}$$

$$\begin{aligned} C_X &= \sum_{n=1}^{N} \frac{F}{T} C_T'' \cos(\theta_n + \alpha_n) - C_{D,off} - \sum_{n=1}^{N} k \frac{F}{T} C_T'' \left[1 - \cos(\theta_n + \alpha_n)\right] \frac{1}{\sqrt{1 + C_T'' \frac{S}{S_P}}} \\ &= C_{D,1} + C_{D,off} + C_{D,3} \end{aligned} \tag{3.3.1}$$

With N, the number of propeller and C_T'' the thrust coefficient of each propeller.

Moreover, beyond these modifications, obtaining an accurate estimation of the power-off lift and drag characteristics of the wing-flap configuration is essential, particularly when experimental data or wind tunnel test results are not available. This necessitates a comprehensive discussion, which is done in the next section, of the methodology employed by ADS to estimate these aerodynamic characteristics.

3.3.2 Power-off : Lift and Drag estimation

Although the methods for estimating the overall drag of an aircraft—encompassing interference drag, induced drag, profile drag, and friction drag—are implemented in ADS and utilized for all subsequent calculations in this work, they will not be detailed here. Similarly,

the estimation methods for lift, which account for 3D effects, fuselage and nacelle influences, Reynolds number effects, and other contributing factors, will also not be exhaustively discussed.

In this section, the focus will be limited to the estimation methods that are significantly influenced by the blown wing effect. To maintain clarity and simplicity, only the lift and drag estimation for the wing-flap configuration will be introduced, under the assumption that the 3D effects of a blown wing aircraft are comparable to those of a conventional aircraft.

Furthermore, this section will identify the inherent limitations of the current approach and explore potential avenues for refinement, ensuring that the methodology remains robust and adaptable to various blown wing configurations.

This discussion will also encompass the determination of operational boundaries related to flap deflection and angle of attack specific to blown wing aircraft. This is crucial for approximating the maximum performance achievable with a given configuration and for ensuring that ADS does not produce values beyond the limits of the method without issuing a warning to the user.

Estimation method for wing-flap characteristics

In the ADS software, the lift and drag characteristics of a known airfoil without flap deflection are determined using XFoil. When flaps are deployed, an increment in both lift and drag is added, following the methods outlined by Roskam in Airplane Design [21]. Specifically, the airfoil lift curve with flaps deflected, illustrated in Fig.3.3.1, is derived through a multi-step process, as detailed in Chapter 8.1 of Airplane Design Part VI. The procedure involves the following key steps:

- A constant increment ΔC_L is applied to the lift curve as a result of flap deflection.
- The lift slope is adjusted to account for the flap chord extension.
- The maximum lift coefficient is estimated based on the modified airfoil geometry.

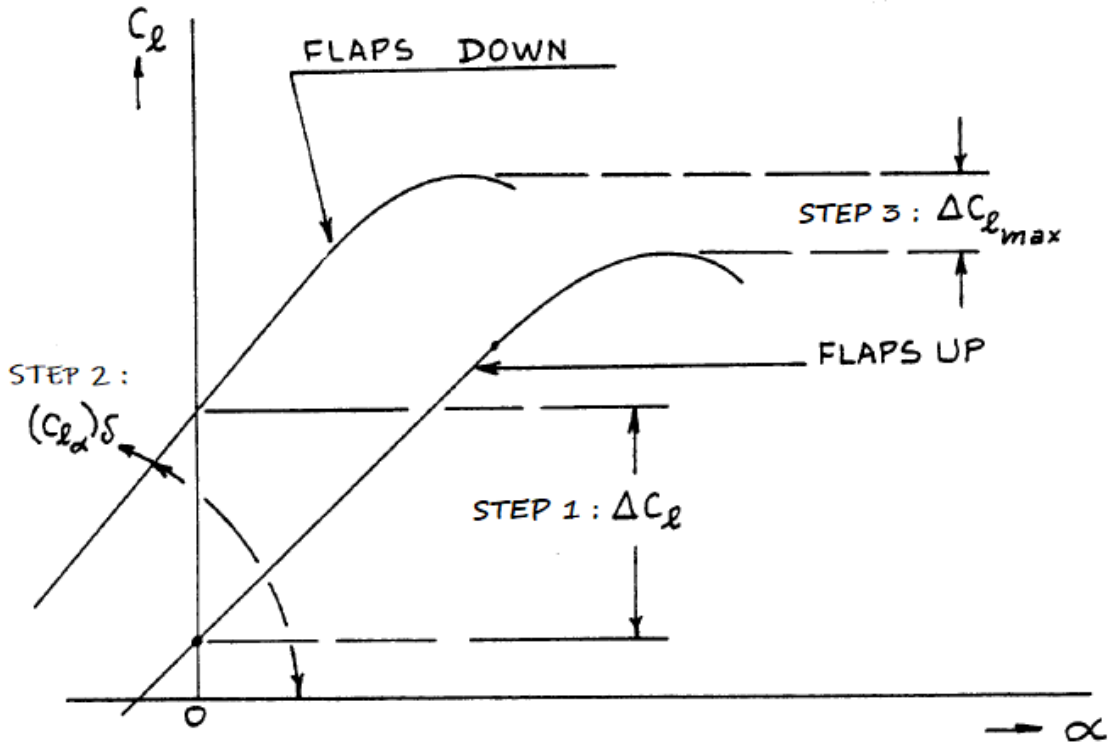

Figure 3.3.1: Multi-Step Flap Lift Increment Method. Extracted and modified from [21]

The accuracy of the estimated lift and drag values depends on several critical parameters, primarily the flap deflection angle, the type of flap used, and the relative chord length of the flap compared to the wing. Assuming no stall conditions, the zero-lift angle of attack and the lift slope are utilized to apply the power-off lift equation **??**.

The drag of the wing-flap configuration is calculated by combining the induced drag with the zero-lift drag of the wing-flap system. The total induced drag is determined using the following equation:

$$C_{D_i} = \frac{C_L^2}{\pi e_0 AR} \tag{3.3.2}$$

Where the Oswald efficiency factor e_0 is computed using the method developed by Nitz and Scholz [24].

The zero-lift drag of the wing-flap configuration is estimated by adding the flap drag increment to the zero-lift drag of the wing. The zero-lift drag increment due to flap deployment is computed according to Chapter 4.6 of Airplane Design Part VI as follows:

$$C_{D,0,flap} = C_{D,p_{flap}} + C_{D,int_{flap}} \tag{3.3.3}$$

Here, $C_{D,p_{flap}}$ represents the profile drag of the flap, while $C_{D,int_{flap}}$ accounts for the

interference drag caused by the flap deployment.

The most significant contributor to this drag is the profile drag, which is primarily influenced by the relative chord length and surface area of the flap compared to the wing, as well as the wing's sweep angle.

Notably, this method has shown an overestimation of profile drag for the Breguet 941 in take-off and wave-off configuration. This discrepancy is likely due to the beneficial effect of the propeller slipstream, which enhances the performance of the flaps. For the Breguet 941's wave-off configuration, a simple correction factor—dependent on the thrust coefficient—was introduced to account for this effect and refine the drag estimation. This correction C_1, applied to the value of the profile drag coefficient of the flap, is defined as :

$$C_1 = \frac{0.5}{0.5 + C'_T} \tag{3.3.4}$$

With C'_T the total thrust coefficient.

However, it is crucial to acknowledge that this correction model has inherent limitations due to its simplicity and reliance on data from a single aircraft type. As a result, the correction is specifically calibrated for the Breguet 941 and may not be directly applicable to other aircraft configurations without further validation and testing.

3.3.3 Stall and Separation Estimation

As previously discussed, the method employed in ADS is valid only within the "unstalled regime" of the wing. However, during the conceptual design phase, it is valuable to estimate the conditions under which separation and stall are likely to occur. Consequently, a threshold indicating the potential onset of separation, as well as the limit of the method's applicability, has been developed. This threshold is based on two primary estimations:

The maximum estimated angle of attack (AOA) before separation at power-off, determined using Prandtl Line theory. For more detailed information, refer to the section on stall speed estimation 5.4.1.

The onset of separation and stall due to flap deflection is estimated using Kuhn's method, as highlighted in subsection 3.2.3.

This threshold is indicated on all comparative graphs in this study, representing the estimated lift curves versus experimental data. The threshold has demonstrated acceptable accuracy, generally underestimating the onset of separation and stall by only a few degrees for the wings analyzed. Furthermore, this threshold also delineates the boundary where correction factors for profile drag and flap efficiency can be applied.

3.4 Limitations of the Developed Method

The simplicity and underlying assumptions of the developed method introduce several limitations, which are explored throughout this work. The impact of these limitations may vary depending on the specific aircraft configuration. For the reader's benefit, these limitations are outlined here, with references to the relevant chapters and sources where applicable.

Limitations Related to Kuhn's Approach

- **Interaction Between Downwash and Slipstream Deflection:** The method assumes no interaction between the propeller slipstream and the overall wing mass flow. In reality, both mass flows interact, resulting in a complex mixing flow that influences the downwash and turning angle. Additionally, the slipstream deflection is based on static conditions and is presumed constant across all speeds.
- **Linear Increase of Slipstream Deflection with Angle of Attack:** The method assumes that the slipstream deflection increases linearly with the angle of attack, which may not accurately reflect real-world conditions.
- **Applicability Restricted to Unstalled Regimes:** The method is only applicable in unstalled flight regimes. Although a procedure to predict flow separation is implemented in ADS, its effectiveness is not fully validated.
- **Fully Developed Slipstream:** The slipstream is assumed to be fully developed at the wing, which may not always be the case in practice.

Limitations Due to Power-Off Estimation

- **Flap Performance Estimation:** Flap performance is estimated using statistical and semi-empirical methods. In reality, the specific design of the flap can significantly affect its performance [21].
- **Complexity in Estimating Flap Profile Drag:** Estimating the profile drag of flaps can be complex, particularly because the propeller slipstream can reduce this drag [**?**], 4.
- **Enhanced Flap Efficiency at High Angles:** The propeller slipstream can lead to enhanced flap efficiency at high angles of attack, which is not fully accounted for in the current method
refChapter4.
- **Lift Distribution Changes:** The changes in lift distribution due to the slipstream are not considered in both the power-off lift and induced drag estimations [19], [20].

Limitations Related to Propeller Design and Position

- **Vertical Position of the Propeller:** The vertical position of the propeller is not considered. Studies suggest that slightly lowering the propeller relative to the wing can enhance the lift characteristics of the system [25], [18].
- **Horizontal Position of the Propeller:** The method does not account for the horizontal position of the propeller. Research indicates that moving the propeller forward can allow the slipstream to develop more effectively, leading to higher lift coefficients [26], [18].
- **Swirl Effects:** The swirl induced by the propeller is not considered. Swirl can increase flow interaction and raise the angle of attack on the upward-moving side of the propeller, potentially causing partial stall of the wing [10].
- **Nacelle Design and Geometry:** Variations in the number and geometry of nacelles are not considered. Nacelles can negatively impact lift distribution and stall characteristics [27], [22].

3.5 Static Stability and Handling capabilities of blown wing aircraft

The static stability of blown wing aircraft is a complex and intriguing topic that still requires extensive research. Additionally, the stability of an aircraft with distributed propulsion is highly dependent on its specific architectural design and thus, will not be fully developed in this work. However, similar to other STOL aircraft, blown wing configurations can encounter significant stability challenges at low speeds [12]. Specifically, the low velocity over the tail can limit the effectiveness of control surface deflections, resulting in diminished control moments. Furthermore, interactions between the propeller slipstream and the control surfaces can critically impact the handling characteristics of a blown wing aircraft.

Given the importance of these issues, it is valuable to briefly introduce certain aspects and characteristics related to the static stability of blown wing aircraft, as well as the design solutions implemented in existing aircraft to address these challenges. Additionally, a method for estimating the pitching moment in blown wing configurations is currently implemented in ADS and will be discussed.

Positive Propulsion-Induced Moments

Several studies have demonstrated the potential of distributed propulsion systems to generate significant yaw and roll moments [28], enhancing handling capabilities at low speeds. However, these moments are often complex due to the coupling effects between thrust and lift. For example, the Breguet 941 utilizes variation in the blade pitch of the outermost propellers

to enhance handling capabilities at low speeds. Similarly, Electra's eSTOL concept leverages blown ailerons to achieve improved roll control by redirecting propeller slipstream.

Longitudinal static stability in Blown Wing Configurations

The pitching moment in blown wing configurations is particularly sensitive to several factors, including flap deflection and thrust coefficient. The mechanisms by which the blown wing influences the pitching moment include:

- **Quarter-Chord Moment Changes Due to Flap Deflection:** High flap deflections can significantly alter the lift distribution, causing the center of pressure to shift rearward[29]. This shift results in changes to the quarter-chord pitching moment, which can complicate the aircraft's longitudinal stability.
- **Thrust-Induced Pitching Moment:** The deflection of the propeller slipstream can also contribute to the pitching moment. More, accurately estimating the location on the wing of the resultant force is challenging, adding further complexity to stability predictions.
- **Slipstream Influence on the tail:** If the tail is positioned within the slipstream, the increased dynamic pressure can substantially affect the aerodynamic characteristics of the control surfaces [30][31]. Additionally, significant downwash effects, resulting from flap deflection, can further complicate the control surface deflection angles needed for stable flight. This downwash varies strongly with the thrust coefficient at low speeds, making it challenging to adapt the control surface deflection angles effectively. Additionally, significant gradients in dynamic pressure have been observed as a function of vertical position relative to the wing, which can drastically change the lift generated by the empennage depending on the aircraft's attitude.

Design Solutions in Existing Blown Wing Aircraft

To address these stability challenges, several design solutions have been implemented in existing blown wing aircraft such as the Breguet 941 and ShinMaywa US-2:

- **Breguet 941:** This aircraft features an all-moving horizontal tail, seemingly placed within the propeller slipstream. The increased dynamic pressure in the slipstream enhances the effectiveness of the horizontal tail and elevators. The horizontal tail and elevator deflections are adjusted according to both thrust coefficient and flap deflection [5].
- **ShinMaywa US-2:** Detailed in the first chapter, this aircraft employs a T-tail configuration to minimize the influence of the slipstream on the tail. To generate sufficient control moments at low speeds, the US-2 uses an internal blowing system that directs high-speed air over all control surfaces. This technology, enabled by a dedicated engine, delays flow separation on the control surfaces and enhances their lift characteristics.

Methodology for Pitching Moment Estimation

Finally, a method has been developed by Obert [32] and later adjusted by Bouquet et al.[33], to calculate the influence of flap deflection, thrust deflection, downwash, and dynamic pressure on the static longitudinal stability of propeller-wing-flap configurations. This method, currently being implemented in ADS, has shown promising initial results for the Breguet 941. However, further investigations are required to validate its applicability to fully blown aircraft configurations.

Chapter 4

Aerodynamic Characteristics of Blown Wing: Experimental and Estimated Values

4.1 Software-Based Replication of 3D Wind Tunnel Experiments

4.1.1 Introduction

In the 1950s, a series of wind tunnel experiments were undertaken at Langley Research Center to investigate the potential and performance of various propeller-wing-flap configurations, specifically in Short Takeoff and Landing (STOL) and Vertical Takeoff and Landing (VTOL) applications. Some of these experiments, with results highlighted in USAF Stability and Control Datcom section 9.2 [34], can served as a basis for validating Kuhn's method.

This section will focus on replicating three of these configurations using the Aircraft Design Software (ADS) to compare the computed lift coefficient and longitudinal force coefficient against the experimental data.

Each configuration's parameters will be detailed, including the test conditions under which they were evaluated. Following this, a brief summary of the authors' key findings from the study will be presented. The results obtained with ADS will be compared to the experimental measurements. This comparison will be followed by a comprehensive discussion on both the experimental and estimated values, delving into the physical phenomena that might explain the experimental results and the discrepancies observed between these and the estimated values.

The first two configurations are sourced from Kuhn, R. E. and Hayes, W. C.[35] and were conducted subsequent to the development of Kuhn's method. Conversely, the third configuration was executed by Kuhn, R. E. and Draper, J.W. [31] before the publication

of his method, suggesting that these results, among others, might have been instrumental in formulating his semi-empirical method and the correction factor "k=1.6". This potential influence may affect the degree of correlation between the experimental and computational results.

4.1.2 Study 1 : Wing equipped with Fowler flap

Experimental overview

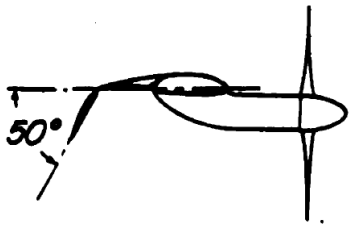

Figure 4.1.1: Sketch of the model [30]

Configuration Characteristics	**Values**
Wing	
Area (S)	5.48 ft^2
Wing chord (c_w)	1.2 ft
Wing chord flap extended (c_we)	1.68 ft
Aspect ratio (AR)	7.66
Airfoil	NACA 4415
Incidence (i_w)	0°
$\frac{c}{D}$	0.85
Camber deflection (δ_e)	7.4°
Propeller	
Number of propeller (N)	4 (no overlap)
Number of blades	3
Diameter (D)	2.0 ft
Rotation speed	5800 rpm
Tip Mac number (M_T)	0.48
Distance from wing leading edge ($d_{LE,prop}$	0.3 D
Flap	
Type	Fowler flap
Flap chord (c_f)	$0.48ft$
$\frac{c_f}{D}$	0.24
Flap deflection (δ)	50°
Flap gap	$0.015c_w$
Flow characteristics	
Slipstream dynamic pressure (q_s)	8 lb/ft^2
Reynolds number slipstream (Re_s)	630 000
Computed values	
Thrust recovery factor ($\frac{F}{T}$)	0.96
Turning angle (θ)	30.96°

Table 4.1.1: Configuration Characteristics extracted from [30],[34].

The data used in this section originates from the study [30]. The investigation was conducted on a half wing equipped with Fowler flaps and sliding flaps, both individually and in combination, including tests performed in and out of ground effect and with or without slats. The moment around the quarter chord was measured for different configurations, and the influence of the slipstream on a fictitious horizontal tail was evaluated. Vanes to measure downwash and dynamic pressure were positioned three wing chords behind the wing at various heights.

The analysis here will concentrate only on the wing with retracted flaps (referred to as the tilted wing) and the wing with the Fowler flap extended to a 50° deflection out of ground effect. The primary characteristics are summarized in Table 4.1.1.

These experiments were performed at a low Reynolds number of 630,000 at zero power and all thrust coefficient. To maintain a constant dynamic pressure in the slipstream across

all thrust coefficients, the free stream velocity was adjusted accordingly. Specifically, for higher thrust levels, the free stream velocity was reduced to ensure the dynamic pressure in the slipstream remained constant. This approach differs from a typical comparison between an aircraft with the wing inside or outside the slipstream, as the dynamic pressure of the flow around the wing would significantly differs in such cases.

However, this setup allows for a focused investigation into the influence of the slipstream on the stall characteristics of the wing, independent of the increase of the dynamic pressure. Specifically, it examines the alteration of flow direction caused by thrust, alongside the increased turbulence and vortex generation within the slipstream.

Key finding

Moment Around Quarter Chord

- A pitching down moment was measured for all flap configurations, which increased with both flap deflection and thrust coefficient.

Downwash and Dynamic Pressure

- Downwash increased with both thrust coefficient and flap deflection.
- Downwash angles of up to 15° were observed at a thrust coefficient of 1.5 for the Fowler configuration deflected at 50°.
- Significant gradients in dynamic pressure (with respect to height) was observed at the fictitious tail position. The maximum dynamic pressure was generally located between 0 and 1 wing chord down relative to the wing.
- High gradients in dynamic pressure may lead to rapid changes in pitching moment with changes in aircraft attitude.
- The results suggest that positioning the tail at a higher location could help mitigate large moment variations due to dynamic pressure gradient and enhance stability.

Stall consideration

- The stall angle increases with the thrust coefficient
- Above the stall angle, the pitching down moment and downash angle decreases drastically till they reach near zero.

Effect of Ground Proximity

- Overall, the ground effect has no impact or a negative impact (that can be larger than 20%) on both lift and drag for all configurations and at all measured heights ($h/D = 0.81, 1.46$).
- Visual observations indicated flow separation occurring on flap at high deflection.
- For the Fowler flap configuration at a 40° deflection, ground effect showed no significant impact on the maximum lift or the lift slope, though the stall became more abrupt. Additionally, drag increased by approximately 10% above 10° of angles of attack.
- The increase of the deflection by the addition of a sliding flap significantly reduced the maximum lift coefficient (C_{Lmax}) in Ground proximity and caused the stall to occur much earlier. There was also a important increase in drag.
- The pitching moment and downwash can be drastically reduce

4.1.3 Experimental and estimated results : Fowler flap retracted

The values of the experimental and estimated forces coefficients and their differences are shown in Fig.4.1.2. The longitudinal force coefficient resulting in a forward acceleration is defined as negative.

As illustrated in Fig.4.1.3a, the lift increases with the thrust coefficient. The experimental angle of attack at which stall occurs also increases with the thrust coefficient, and the stall becomes less abrupt.

The discrepancies between the experimental and estimated values of the lift and drag coefficients are depicted in Fig.4.1.3b, Fig.4.1.2d and remain within acceptable limits up to near the stall angle. The line at $AOA = 15°$ represents the stall angle estimated by ADS based on the method detailed in the section concerning V_min. This estimation serves as an indication of the boundary of the method's applicability and appears to closely approximate the stall angle for lower thrust coefficients.

The drag polars, presented in Fig.4.1.3, are derived by adding the thrust coefficient to the longitudinal force coefficient. These drag polars demonstrate that blowing the wing enables the achievement of significantly higher lift coefficients (with the cost of higher lift-to-drag ratio) than the unblown wing.

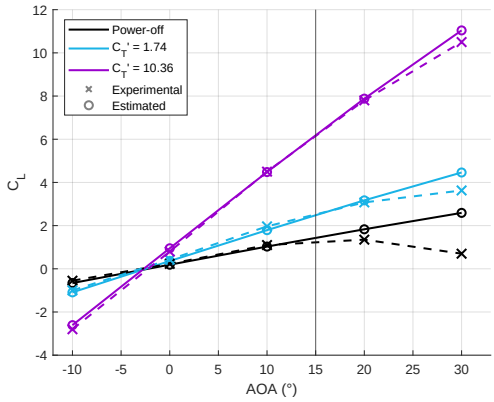

(a) Lift coefficient vs angle of attack.

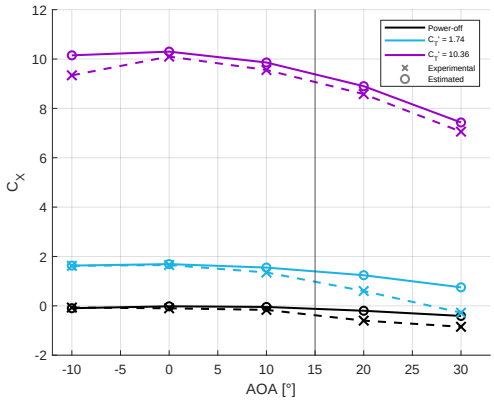

(b) Longitudinal force coefficient vs. angle of attack.

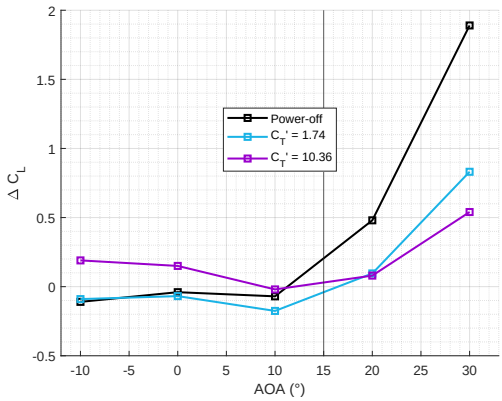

(c) Difference between lift coefficient estimated and experimental value vs. angle of attack.

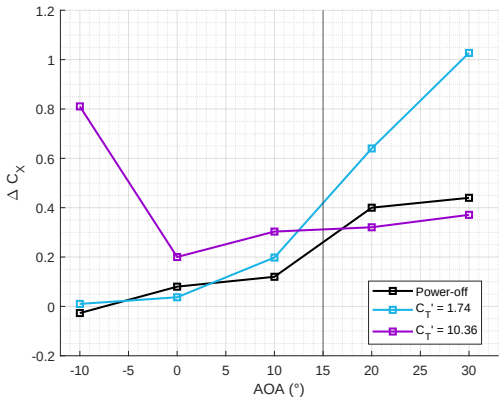

(d) Difference between longitudinal force coefficient estimated and experimental value vs. angle of attack.

Figure 4.1.2: Force coefficients estimated and experimental values for various thrust coefficients. Estimated stall angle 15°. Flap retracted, $Re_s = 630\,000$.

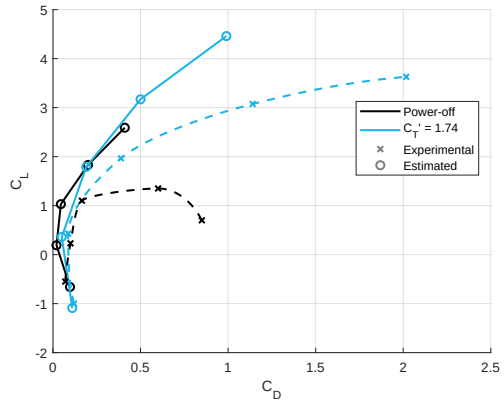

(a) Power off and Medium thrust coefficient.

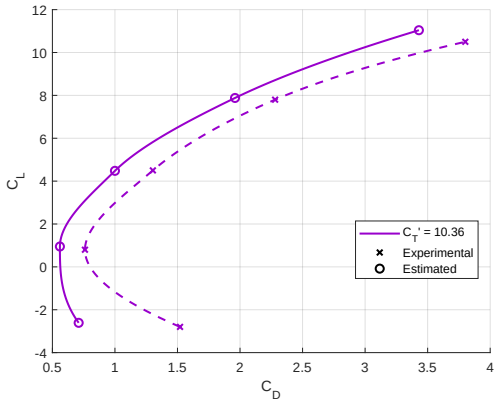

(b) High thrust coefficient.

Figure 4.1.3: Estimated and experimental drag polar for various thrust coefficients. Flap retracted, $Re_s = 630\,000$.

Experimental and estimated results : Fowler flap deflected at $50°$

The values of the experimental and estimated force coefficients and their differences are depicted in Fig.4.1.1. Relative errors are shown in Fig.4.1.5 and drag polars in Fig4.1.6. The trends observed are similar to those of the wing without flaps with some additional observations.

Key observations

- Both longitudinal force coefficient and lift coefficient increase with thrust coefficient.
- The maximum difference in lift coefficient at power-on and out-of-stall conditions is 0.1 (refer to Fig. 4.1.4b), which corresponds to a relative error of less than 5% (refer to Fig. 4.1.9a).
- There is a noticeable increase in errors attributable to the longitudinal force as shown in Fig4.1.4d. The maximum difference is $\Delta C_x = 0.3$ and appears at an angle of attack of $10°$ for a thrust coefficient of 0.92. This is equivalent to an error of 18% relative to the thrust coefficient (refer to Fig. 4.1.9b).
- The observed turning angle was around $30.96°$ while the maximum turning angle achievable estimated with the Kuhn's method was $28.5°$.
- The drag polars shown in Fig.4.1.6 indicate an overestimation of the lift-to-drag ratio.

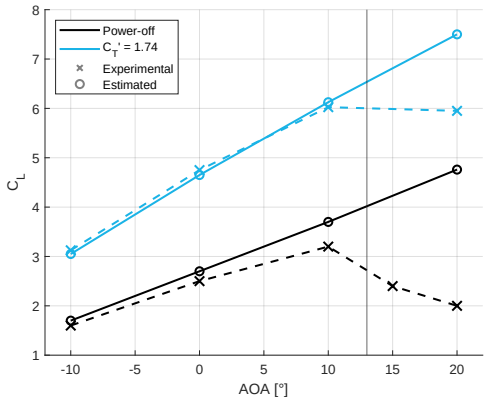

(a) Lift coefficient vs. angle of attack.

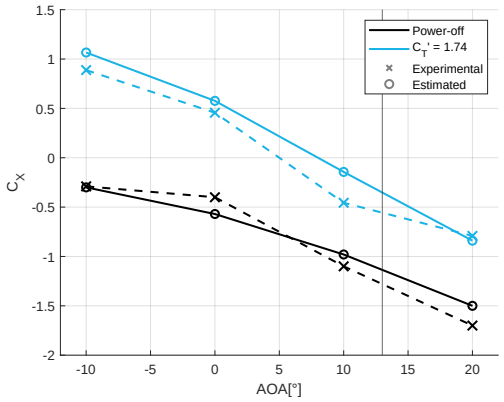

(b) Longitudinal force coefficient vs. angle of attack.

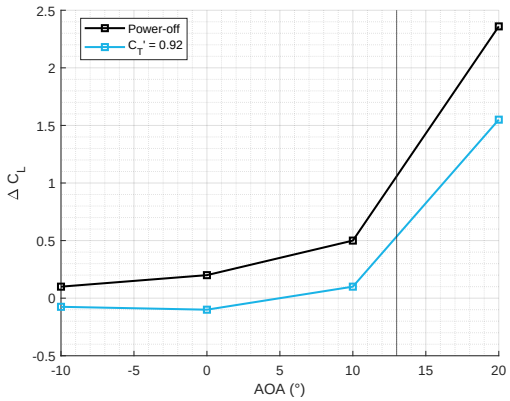

(c) Difference between lift coefficient estimated and experimental values vs. angle of attack.

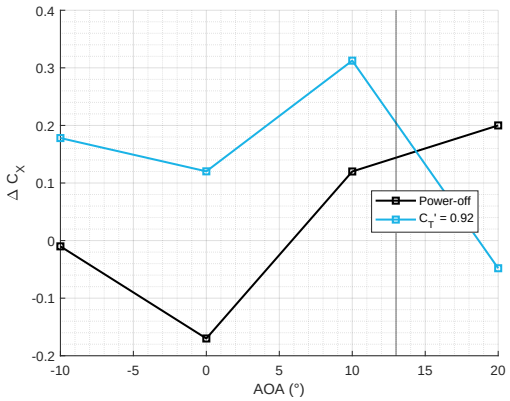

(d) Difference between longitudinal force coefficient estimated and experimental values vs. angle of attack.

Figure 4.1.4: Force coefficients estimated and experimental values for various thrust coefficients. Estimated stall angle 13°. Fowler flap deflected at 50°, $Re_s = 630\,000$

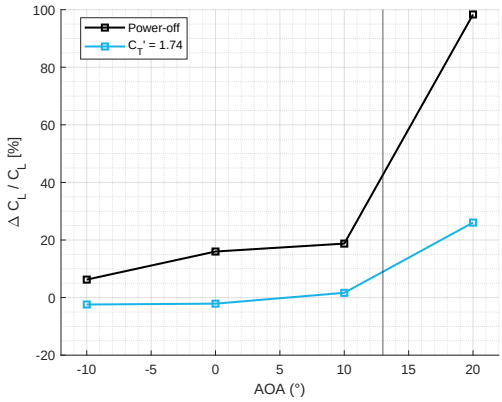

(a) Lift coefficient relative error vs. AOA.

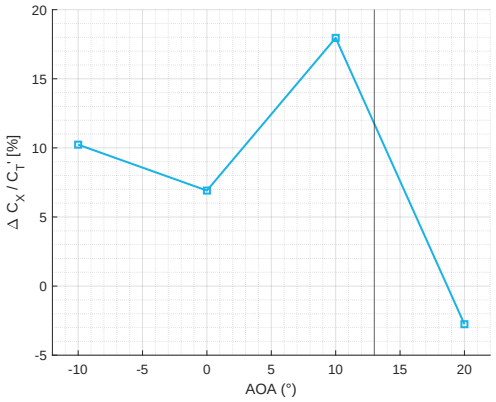

(b) Longitudinal force coefficient relative error vs. AOA.

Figure 4.1.5: Relative errors (express in percent) as a function of angle of attack. The error in lift coefficient is shown relative to experimental lift coefficient, while the error in longitudinal force coefficient is shown relative to the thrust coefficient. Fowler flap deflected at 50° , $Re_s = 630\,000$.

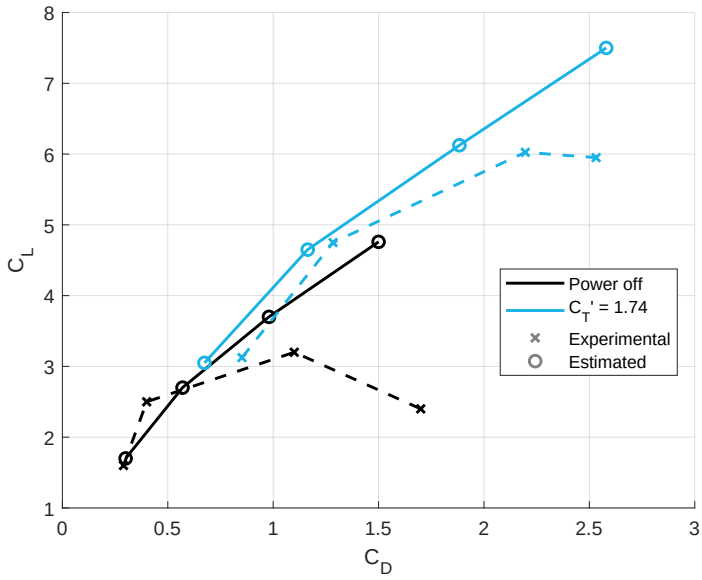

Figure 4.1.6: Estimated and experimental drag polar for various thrust coefficients. Fowler flap deflected at 50° , $Re_s = 630\,000$.

4.1.4 Study 2 : Wing with Slotted flap

The data used in this section originates from the study [31]. The study was conducted on a half wing equipped with slotted flaps.

The analysis here will concentrate only on the wing with a single slotted flap with a

50-degree deflection. The primary characteristics are summarized in Table 4.1.2.

These experiments were performed at a low Reynolds number of 800 000. Similarly to the first configurations, the dynamic pressure in the slipstream was maintained across all thrust coefficients, the free stream velocity was adjusted accordingly. This approach differs from a typical comparison between an aircraft with the wing inside or outside the slipstream.

Experimental overview

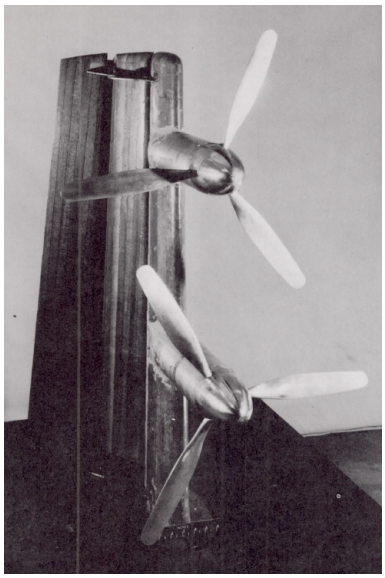

Figure 4.1.7: Model of the wing [31]

Geometric Characteristics	**Details**
Wing	
Area	5.125 ft^2
Mean aerodynamic chord	1.514 ft
Airfoil section	NACA 0015
Aspect ratio	4.55
Taper ratio	0.714
Propellers	
Number of propeller	2
Diameter	2.0 ft
Nacelle diameter	0.33 ft
Airfoil section	Clark Y
Flap	
Type	Slotted flap
Flap chord (c_f)	0.45 ft
$\frac{c_f}{D}$	0.226
Flap deflection (δ)	60°
Flow characteristics	
Slipstream dynamic pressure (q_s)	8 lb/ft^2
Reynolds number slipstream (Re_s)	800 000
Additional values	
Thrust recovery factor ($\frac{F}{T}$)	0.96
Turning angle (θ)	28.2°

Table 4.1.2: Configuration characteristics extracted from [31].

Key finding

Similar conclusions to those of the first study were drawn, with an additional key observation:

- Increasing the thrust coefficient not only elevates the angle of attack at which maximum lift occurs but also reduces the variation in the lift coefficient at angles of attack beyond the maximum lift angle. This suggests that higher thrust coefficients contribute to a more stable aerodynamic performance by moderating the changes in lift at higher angles of attack.

Experimental and estimated results : Slotted flap deflected at $60°$

The estimated and experimental force coefficients and their differences are presented in Figure 4.1.8, while the relative errors are shown in 4.1.9 .The drag polars can be found in Figure 4.1.10.

As shown in Fig.4.1.8a the stall angle, or the angle at which the maximum lift coefficient occurs, increases with the thrust coefficient. The estimated stall angle (defined in the section relative to the V_{min}) is 11 degrees, and as shown in Fig.4.1.8b, the lift estimations remain accurate within an acceptable margin up to this angle. At higher thrust coefficients, the lift coefficient is underestimated, suggesting that the effectiveness of the flaps improves with increased thrust.

Key observations

- The maximum error in the lift coefficient is -0.6 and occurs at zero angle of attack for $C'_T = 1.43$. This corresponds to a relative error of approximately 20%.
- The longitudinal force coefficient is inaccurately estimated, especially at high thrust coefficients. The maximum error outside of stall conditions is around 0.38, corresponding to a relative error of approximately 25%.
- The measured turning angle is $28.2°$, whereas the maximum estimated turning angle for this configuration is $27.2°$.
- The experimental drag polar is highlighted in Fig. 4.1.10a to illustrate the various achievable lift-to-drag ratios. The figure demonstrates that higher lift-to-drag ratios can be achieved with higher thrust coefficients for a given lift coefficient.

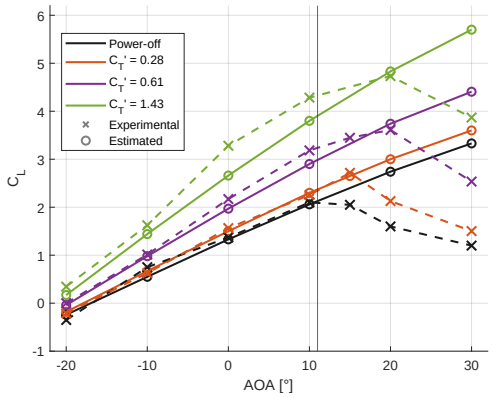

(a) Lift coefficient vs. angle of attack.

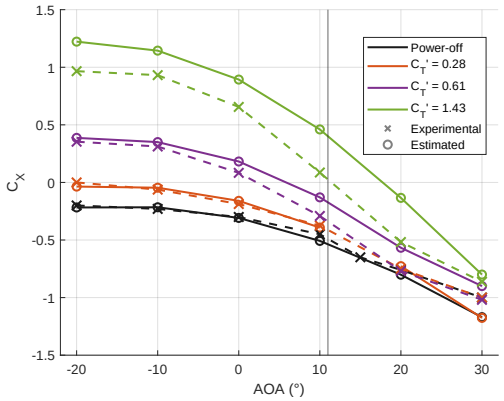

(b) Longitudinal force coefficient vs. angle of attack.

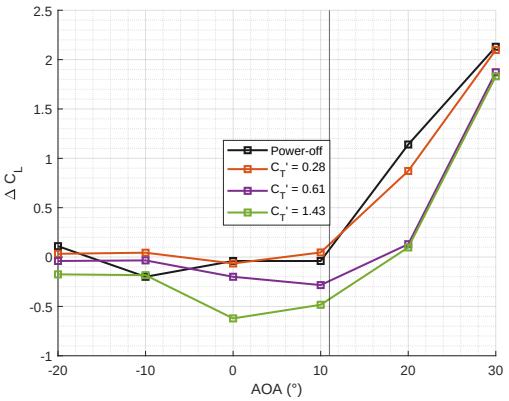

(c) Difference between lift coefficient estimated and experimental values vs. angle of attack.

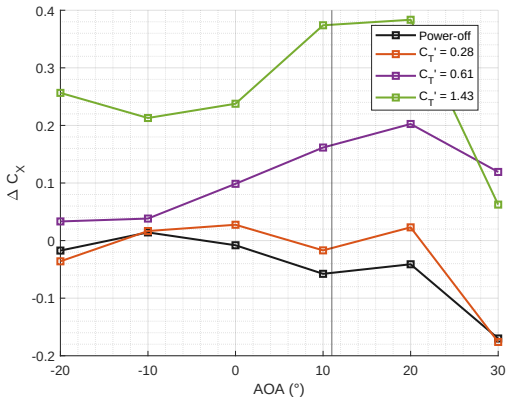

(d) Difference between longitudinal force coefficient estimated and experimental values vs. angle of attack.

Figure 4.1.8: Force coefficients estimated and experimental values for various thrust coefficients. Estimated stall angle 11°. Slotted flap deflected at 60°, $Re_s = 630\,000$

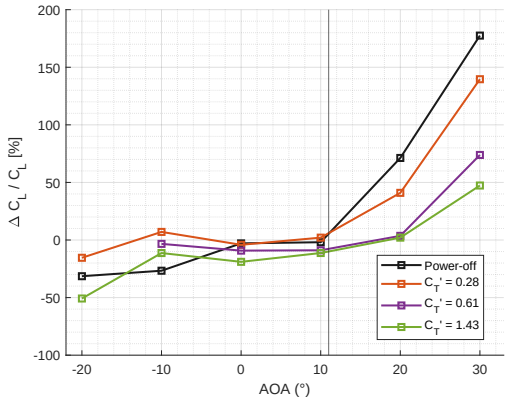

(a) Relative error in lift coefficient vs. angle of attack.

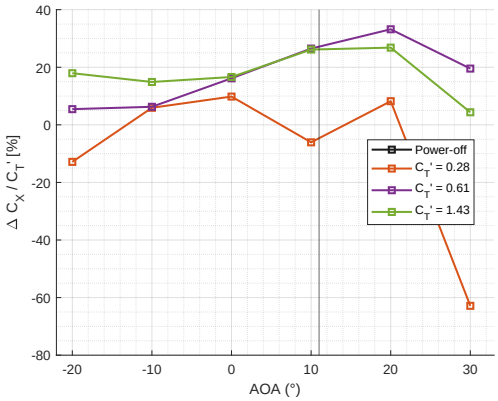

(b) Relative error in longitudinal force coefficient vs. angle of attack.

Figure 4.1.9: Relative errors (express in percent) as a function of angle of attack. The error in lift coefficient is shown relative to experimental lift coefficient, while the error in longitudinal force coefficient is shown relative to the thrust coefficient. Slotted flap deflected at 60° , $Re_s = 800\,000$.

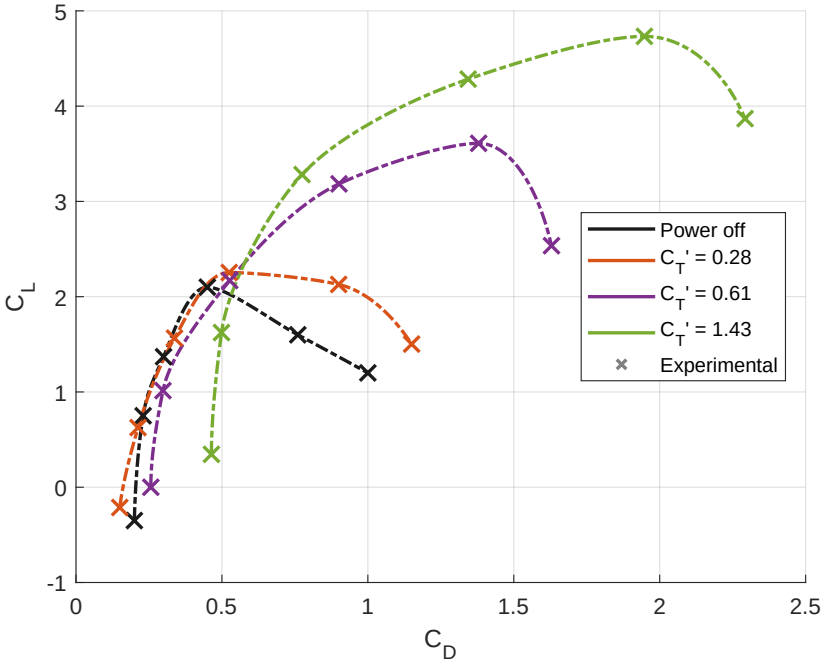

(a) Experimental drag polar (with interpolation) for various thrust coefficient.

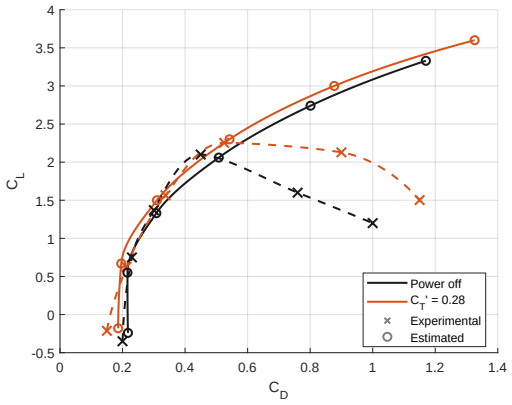

(b) Experimental and estimated drag polar : Low thrust coefficient.

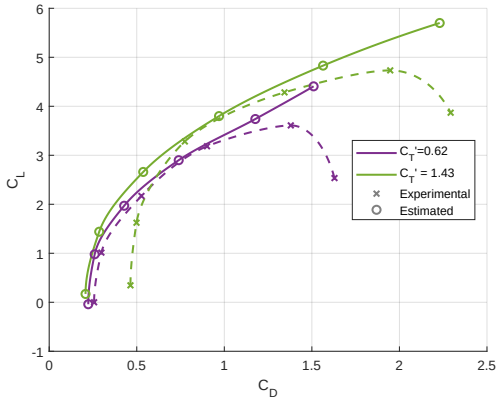

(c) Experimental and estimated drag polar : Medium thrust coefficient.

Figure 4.1.10: Estimated and experimental drag polar for various thrust coefficients. Slotted flap deflected at 60° , $Re_s = 800\,000$.

4.1.5 Interpretation of results and Discussion

Overall, the lift coefficient is accurately estimated (generally within $5 - 15\%$ error) up to the point of stall. It is clearly observed that the stall angle of attack increases with the thrust coefficient, even when the slipstream dynamic pressure of the flow remains constant. This indicates that an increase in dynamic pressure is not the sole factor contributing to the delay of stall in blown wing configurations. The redirection of flow caused by thrust and the possible facilitation of flow transition from laminar to turbulent by the propeller may play significant roles. Indeed, the formation of a turbulent boundary layer could help to delay the onset of stall. It is also observed that the lift coefficient for the slotted flap increases drastically with the thrust coefficient, even exceeding the estimations. This phenomenon can likely be explained by the improved airflow around the wing facilitated by the slipstream.

The longitudinal force coefficient is overestimated in most cases, particularly at high thrust coefficients. Wings with deflected flaps generally exhibit a drag error outside of stall conditions ranging from 0.1 to 0.4 Cd. This error, when considered relative to the thrust coefficient, typically falls between 5% and 30%. In practical terms, this means that, in the worst-case scenario, there would need to be a 30% (relative to the thrust) increase in the longitudinal force to align with the experimental values. This discrepancy can be attributed to the significant flap deflection, which results in a turning angle that exceeds the computed maximum turning angle achievable for this type of flap, estimated by Kuhn's method. Beyond this maximum angle, the relationship between flap deflection and turning angle becomes nonlinear, flow separations and/or bursting of the wake occur and lead to significant increase in drag. For the slotted flap, the notion is supported by the study's explicit observation: "The lift and pitching-moment data for a deflection of 40° are seen to be almost the same as for a deflection of 60° ... Increasing the flap deflection from 40° to 60° results mainly in a decrease in the longitudinal-force coefficient."[31]. Furthermore, Richard E. Kuhn later applied his method to the same wing, this time with a plain flap deflected at a modest 30°. The analysis revealed that the longitudinal force coefficient was estimated with an error margin of less than 5% of the experimental data. The detailed results of this evaluation are documented at the conclusion of the NASA MEMO outlining his methodology [3].

These observations also indicate that higher lift-to-drag ratios could be attained by reducing the deflections of these flaps. Nevertheless, these configurations remain relevant as they provide crucial insights into achievable deflection angles and stall characteristics. During approach, blown wing aircraft necessitate substantial drag force to compensate the thrust. Consequently, it is essential to use flap deflection angles that generate high drag without the risk of stall. The results demonstrate that for high thrust coefficients, stalls are not abrupt, and increasing the angle of attack beyond the stall angle continues to produce significant lift while dramatically increasing drag. This characteristic is advantageous as it ensures deceleration without compromising lift.

Next, it is important to note that the experimental conditions, specifically using a constant dynamic pressure in the slipstream, do not represent the variations that would occur for an aircraft with different thrust coefficients. An increase in thrust would significantly raise the dynamic pressure and slipstream velocity. This elevation would energize the boundary layer, thereby limiting flow separation on the wing and flaps. Consequently, this would potentially

result in a higher stall angle of attack and an improved lift-to-drag ratio for the wing with substantial flap deflections.

Finally, it is evident that the method developed in this study has its constraints and cannot capture the variations in flow characteristics associated with different thrust coefficients. Specifically, these constraints become more apparent near stall conditions, which can result from excessively high angles of attack or significant flap deflections. In such scenarios, the method's ability to accurately predict aerodynamic forces diminishes due to the complex interactions within the flow. Moreover, the conditions for blown wing stall are challenging to define accurately without wind tunnel experiments or extensive computational simulations. Nevertheless, the stall angle of attack determined by ADS and the maximum turning angle serve as effective boundaries. Within these limits, the method provides rapid estimations with a relatively low margin of error, making it particularly suitable for conceptual design phases.

4.2 Breguet 941

4.2.1 Introduction

This section provides a detailed analysis and comparison of the lift curve and drag polar estimations for the Breguet 941 aircraft, using data derived from NASA flight tests.

A distinctive characteristic of the Breguet 941, as with any aircraft employing a blown wing system, is that the lift curve and drag polar are significantly influenced by the thrust. Consequently, the results are presented for various thrust coefficients to capture the full scope of this interaction.

The study focuses on three specific inboard/outboard flap deflections δ_f: 45/30, 75/50, and 98/65, which correspond to the Take-off, Wave-off, and Landing configurations of the Breguet 941, respectively. The lift curve and longitudinal force coefficient-Polar, cross plotted from flight test and available in [5] are shown inFig.4.2.1. The longitudinal force coefficient, $\overline{C_D}$ or C_X resulting in a forward acceleration is defined as negative.

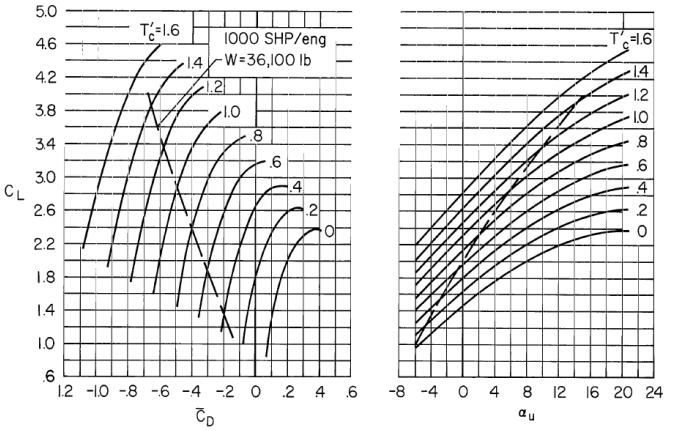

(a) Take-off configuration ; $\delta_f = 45/30$.

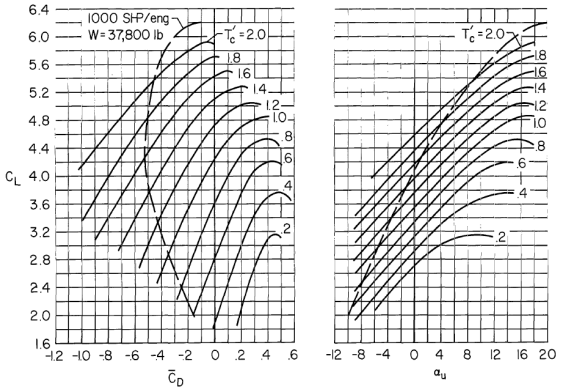

(b) Wave-off configuration; $\delta_f = 75/50$.

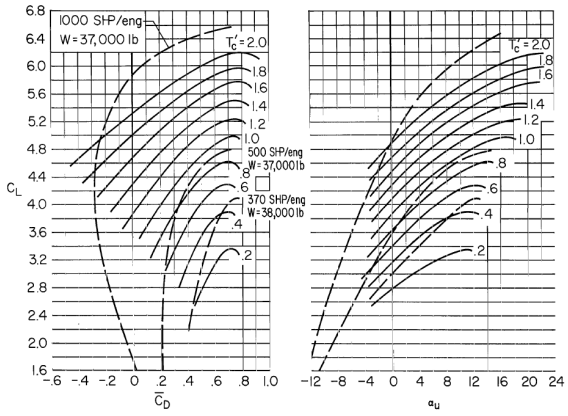

(c) Landing configuration ; $\delta_f = 98/65$.

Figure 4.2.1: Lift Curve and Longitudinal Force-Polar Variation with Various Thrust Coefficients ($T_c' = C_T'$), extracted from [5]. The angle of attack indicated here requires a correction (calibration available in [5]). The true value depends on the configuration but can be approximated by $\alpha = (0.73 \times \alpha_i) - T_c'$.

Overall, the analyses reveal some differences between the model predictions and the flight test results. These discrepancies are primarily attributed to the treatment of the drag increment due to flaps in the "power-off" component of the estimation method.

Upon further investigation, it was observed that drag was significantly overestimated in all configurations. In the Take-off configuration, this overestimation was found to be a constant value across all angles of attack before stall and for all thrust coefficients. By analyzing the experimental power-off drag polar in the Take-off configuration, it was estimated that the aircraft's zero-lift drag coefficient ranged between 0.03 and 0.07. However, ADS provided a zero-lift drag coefficient of 0.30, with 0.25 attributed to the profile drag of the flaps. This overestimation likely results from the method assuming double-slotted flaps, whereas the Breguet 941 features two main element flaps with a small fixed "airfoil-like" element in between. These flaps were specifically designed to optimize the wing's performance in the Take-off configuration. The flap profile drag coefficient was thus reduced by 0.2.

A similar observation was made for the Wave-off configuration, where drag was consis-

tently overestimated across pre-stall angles of attack. However, in this case, a correlation was observed between the thrust coefficient and the drag discrepancy. This correlation is physically plausible, as it has been shown that the slipstream can mitigate potential separations that might occur without the influence of the slipstream.

To address these discrepancies, a simple correction model that adjusts the flap profile drag is proposed:

$$C_{D,f,p,\text{corrected}} = C_1 \times C_{D,flap,p}$$

where $C_{D,flap,p}$ is the profile drag of the flap, and C_1 is the correction factor defined as:

$$C_1 = \frac{0.5}{0.5 + C'_T}$$

This model aims to explore the relationship between thrust coefficient and flap drag, refining the accuracy of the predictions. However, it is important to note that the correction model is based on data from the Wave-off configuration. Therefore, the fit of the correction is specifically tailored to the Breguet 941 and may be biased due to potential errors in the overall method.

The Landing configuration also posed several challenges due to the extremely high flap deflection, which exceeds the limits of all available semi-empirical estimation methods. These formulas generally stop at deflections of $60 - 70$ degrees, so the values at these limits were chosen for the inboard propellers. Additionally, the flap deflection results in a theoretical θ that exceeds the maximum possible θ estimated by Kuhn's method, likely indicating some flow separation on the upper surface of the wing. Therefore, no correction to the profile drag was applied, as this configuration clearly falls outside the limits of the method. The computed turning angle was also constrained to the maximum turning angle to more closely approximate the real value. This adjustment allows for a better evaluation of whether Kuhn's approach accurately determines the limitations associated with flap deflection. The results and their interpretation regarding the landing configuration are limited due to the complexity of the configuration.

The results presented in this section were obtained under the assumption of level flight, where lift equals weight. To accurately replicate the flight test conditions conducted by NASA, the specific parameters of each test, including altitude (and therefore air density), aircraft speed, weight, thrust coefficient, and angle of attack, were meticulously input into the ADS software. This careful replication ensures that the simulations closely match the actual flight conditions.

More, the contributions of each term in the lift and longitudinal force equations were analyzed for various flight conditions. These contributions are highlighted in the results to help the reader understand the different implications of the configurations studied. For clarity, the simplified equations are restated here. It is also important to note that a longitudinal force resulting in a forward force is defined as NEGATIVE in the drag and C_X polar. Therefore,

a minus sign ("-") is introduced in this specific C_X equation.

$$C_L = C_{L,off} + \frac{F}{T}C'_T \sin(\theta+\alpha) + k\frac{F}{T}C'_T \sin(\theta+\alpha)\frac{1}{\sqrt{1+\frac{C'_T S}{NS_p}}}$$

$$= C_{L,off} + C_{L,2} + C_{L,3}$$

$$-C_X = \frac{F}{T}C'_T \cos(\theta+\alpha) - C_{D,off} - k\frac{F}{T}C'_T\left[1-\cos(\theta+\alpha)\right]\frac{1}{\sqrt{1+C'_T\frac{S}{NS_P}}}$$

$$= C_{X,1} + C_{D,off} + C_{X,3}$$

Finally, the results for the take-off and wave-off configurations are presented both with and without the applied corrections, providing a clear comparison of the potential outcomes in the absence of these adjustments. It is important to note that the initial and final points of the drag polar curves differ between the experimental and estimated values. This discrepancy arises because the estimations begin at a zero angle of attack and typically extend up to around 15 degrees, whereas the experimental data often start at angles significantly below zero and frequently stop at lower angles.

4.2.2 Take-off configuration

The lift curves, both estimated and experimental, for various thrust coefficients are presented in Fig.4.2.2. Overall, the estimated lift values align well with the experimental data within the unstalled regime. The limit of the unstalled regime is estimated thanks to ADS method (refer to 5.4.1).

However, there is an observed overestimation of approximately 0.17 in the lift coefficient at zero angle of attack under power-off conditions. Additionally, there is a slight underprediction of the overall lift slope across all thrust coefficients, indicating a potential discrepancy in the linearity of the lift response as modeled by the estimation method.

The longitudinal force and drag polar curves are depicted in Fig.4.2.3b. As previously discussed, the profile drag coefficient associated with flap deflection under power-off conditions was initially overestimated by 0.2. To address this, a correction has been applied, and the results are presented both with and without this adjustment. Despite the correction, the drag polar still shows deviations from the experimental data at higher thrust coefficients. Conversely, the corrected drag polar closely matches the experimental values at lower thrust coefficients, indicating a more reliable performance of the model under these conditions.

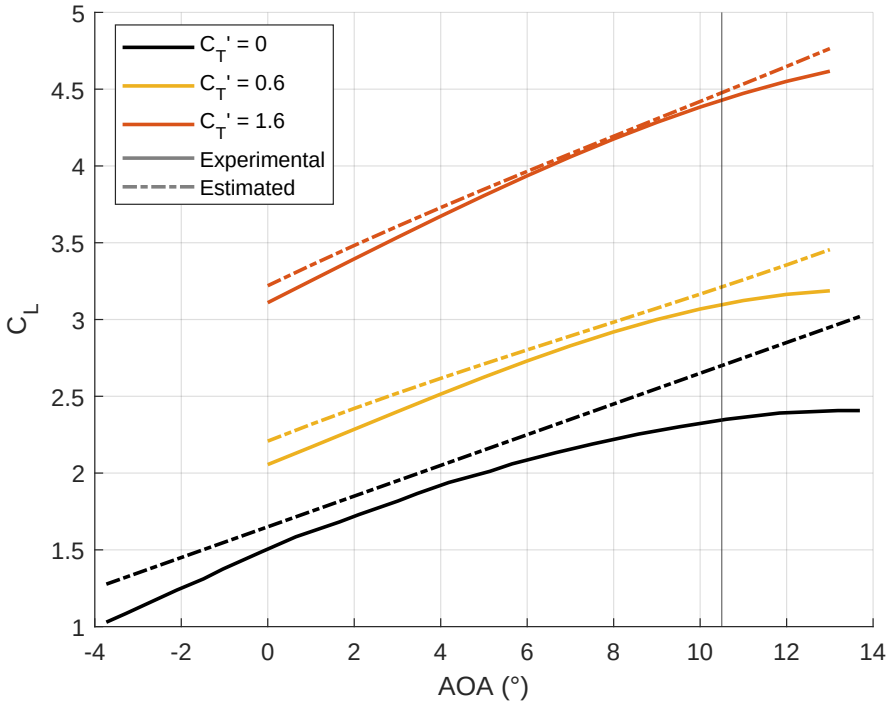

Figure 4.2.2: Lift curve for various thrust coefficient in Take-off configuration ($\delta_f = 45/30$) : Estimated vs Experimental values. The horizontal line at $\alpha = 10.5$ represents the end of the unstalled regime computed by ADS.

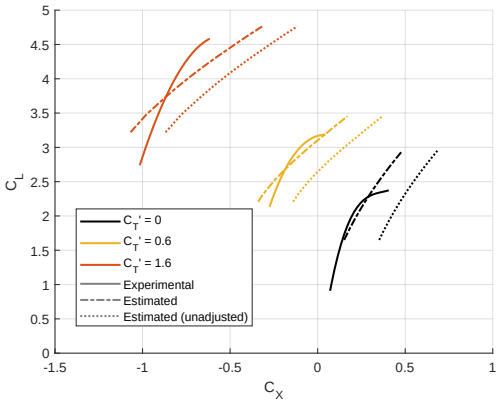

(a) Longitudinal Force Coefficient Polar.

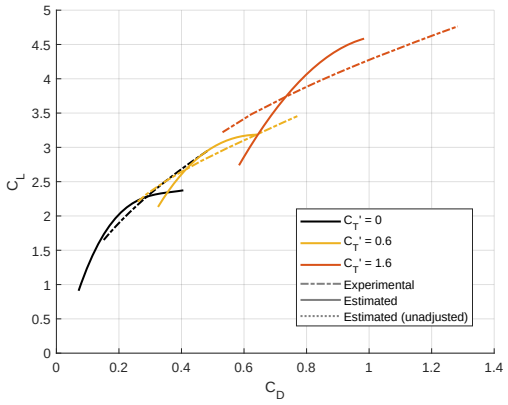

(b) Drag Polar ; the drag is obtained by subtracting C'_T from $\mid C_X \mid$

Figure 4.2.3: Longitudinal Force Polar an Drag polar Variation with Various Thrust Coefficients (C'_T) in Take-off configuration ($\delta_f = 45/30$) : Estimated vs Experimental values. The estimated values are presented with and without the correction on flap profile drag. The experimental values are extracted from [5] and based on flight test data

For a specific flight condition characterized by a thrust coefficient of 1.6 and a zero angle of attack in the Take-off configuration, the estimated values are summarized in Table **??**.

This table highlights the key aerodynamic parameters and contributions to the overall lift and drag. The analysis reveals that a lift coefficient of 3.2 is achieved that approximately half of the total lift is derived directly from the lift associated with the blown wing effect. However, this increase in lift comes at the cost of a deflected thrust and an additional drag of 0.46, reducing significantly the longitudinal force.

Configuration Characteristics	**Values**
Flight Condition	
Total thrust coefficient (C'_T or T'_C)	1.6
Altitude	5000 ft
Weight (W)	37 500 lbs
Center of Gravity position in % of wing chord	30.5%
Flight speed	$\sim$ 63 knots
Angle of attack (α)	0°
Reynolds number based on mean c_w (Re)	$\sim$ 7 200 000
Estimated parameters	
Înboard slipstreams Turning angle (θ_1)	38.4°
Înboard Maximum Turning angle ($\theta_{1,MAX}$)	47.5°
Outboard slipstreams Turning angle (θ_2)	24.4°
Outboard Maximum Turning angle ($\theta_{2,MAX}$)	35.1°
Thrust recovery factor ($\frac{F}{T}$)	0.98
Estimated Lift coefficient	
Total lift coefficient (C_L)	3.21
Power-off lift ($C_{L,off} = C_{L,wing} + \Delta C_{L,flap}$)	1.68
Power-off wing-flap lift slope ($C_{L,\alpha}$)	5.7 per radian
Power-off Wing lift ($C_{L,wing}$)	0.48
Power-off Flap lift increment ($\Delta C_{L,flap}$)	1.2
Lift due to deflected thrust ($C_{L,2}$)	0.87
Lift due to mass flow increase ($C_{L,3}$)	0.66
Estimated Longitudinal force coefficient	
Total Longitudinal force coefficient (C_X)	-0.97
Longitudinal force due to thrust ($C_{X,off}$)	-1.34
Power-off drag ($C_{X,off} = C_{D,i} + C_{D,0}$)	0.17
Power-off induced drag ($C_{D,i}$)	0.09
Power-off zero lift drag ($C_{D,0}$)	0.08
Power-on induced drag ($C_{X,3}$)	0.20

Table 4.2.1: Key Example: Flight condition and estimated values at $C'_T = 1.6$ and $\alpha = 0°$, in Take-off configuration.

4.2.3 Wave-off configuration

The lift curves, both estimated and experimental, for various thrust coefficients are presented in Fig.4.2.4. The estimated lift values demonstrate overall good alignment with the experimental data within the unstalled regime, particularly at medium and high thrust coefficients.

However, the estimated limit of angle of attack appears to be overestimate at low thrust coefficients. Experimentally, a maximum lift coefficient of 5.5 is achieved with a thrust coefficient of 1.6.

Across all thrust coefficients and unstalled angles of attack, there is a consistent slight underestimation of lift. This discrepancy, up to 10%, appears to be primarily due to the underestimation of the power-off lift contribution. Similar to the take-off configuration, the overall lift slope is slightly underpredicted across all thrust coefficients.

The longitudinal force and drag polar curves, depicted in Fig.4.2.5, further illustrate the aerodynamic characteristics under wave-off conditions. As previously discussed, the initial estimation of the profile drag coefficient associated with flap deflection under power-off conditions was found to be overestimated. Unlike the take-off configuration, where the flap profile drag seemed unaffected by changes in thrust coefficient, the wave-off configuration exhibited a reduction in flap profile drag as the thrust coefficient increased. To account for this observation, a correction factor, dependent on the thrust coefficient, was applied. It is demonstrated that by using this correction factor, the estimated lift-to-drag ratio values closely match the experimental results.

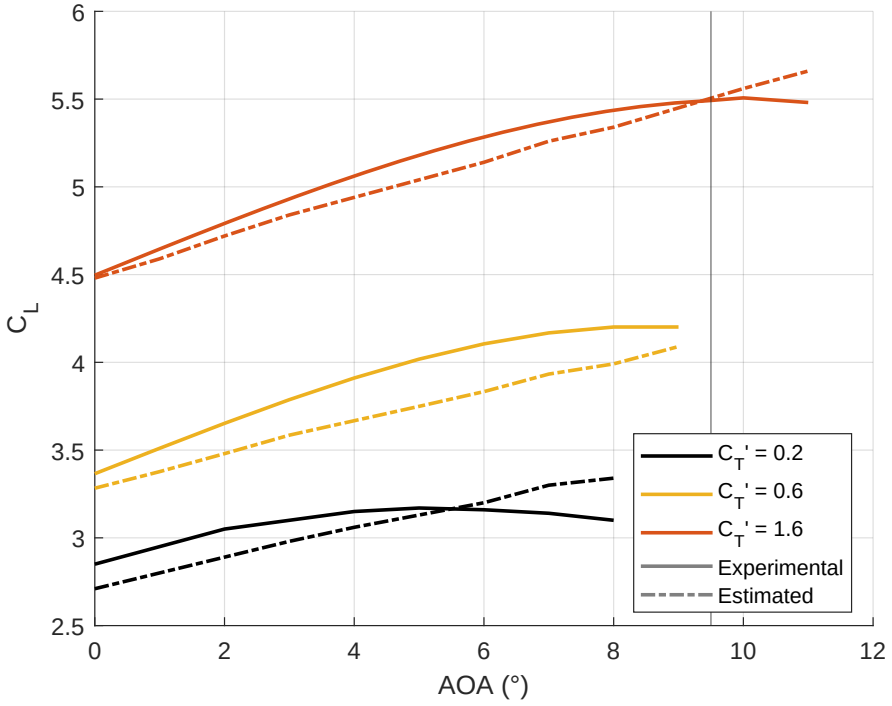

Figure 4.2.4: Lift curve for various thrust coefficient in Wave-off configuration ($\delta_f = 75/50$) : Estimated vs Experimental values. The horizontal line at $\alpha = 9.5$ represents the end of the unstalled regime computed by ADS.

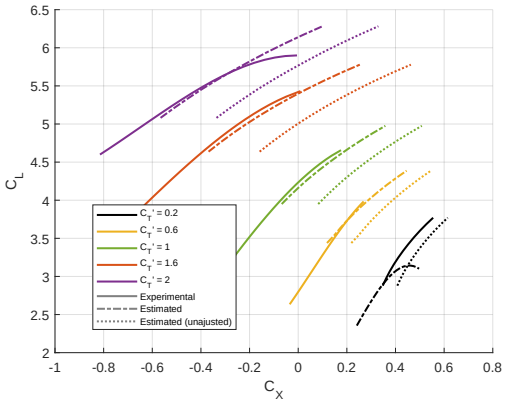

(a) Longitudinal Force Coefficient Polar.

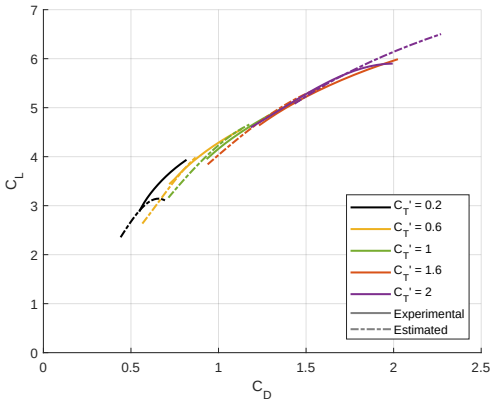

(b) Drag Polar ; the drag is obtained by adding C'_T to C_X

Figure 4.2.5: Longitudinal Force Polar an Drag polar Variation with Various Thrust Coefficients (C'_T) in Wave-off configuration ($\delta_f = 75/50$) : Estimated vs. Experimental values. The estimated values are presented with and without the correction on flap profile drag. The experimental values are extracted from [5] and based on flight test data

The estimated values for a specific flight condition (thrust coefficient equal to 1.6 and at zero angle of attack) in the wave-off configuration are illustrated in Table 4.2.2, highlighting various key values and parameters. It is shown that, compared to the standard take-off configuration, the lift is increased due to both power-off flap lift increment and slipstream deflection. More than half of the lift is directly attributable to slipstream deflection. However, this increase in lift is achieved with greater thrust deflection, resulting in a worse lift-to-drag ratio.

It is also calculated that the estimated turning angle is very close to the maximum possible turning angle of these flaps, as established by Kuhn. This maximum turning angle is even slightly exceeded by the inboard flaps, suggesting that these flaps cannot be further deflected without causing separation. This hypothesis is supported by the results from the landing configuration.

Configuration Characteristics	Values
Flight Condition	
Total thrust coefficient (C'_T or T'_C)	1.6
Altitude	5000 ft
Weight (W)	37 500 lbs
Center of Gravity position in % of wing chord	30.5%
Flight speed	$\sim$ 53 knots
Angle of attack (α)	0°
Reynolds number based on mean c_w (Re)	$\sim$ 6 040 000
Estimated parameters	
Înboard slipstreams Turning angle (θ_1)	50.8°
Înboard Maximum Turning angle ($\theta_{1,MAX}$)	47.5°
Outboard slipstreams Turning angle (θ_2)	36.6°
Outboard Maximum Turning angle ($\theta_{2,MAX}$)	35.1°
Thrust recovery factor ($\frac{F}{T}$)	0.98
Estimated Lift coefficient	
Total lift coefficient (C_L)	4.5
Power-off lift ($C_{L,off} = C_{L,wing} + \Delta C_{L,flap}$)	2.28
Power-off Wing lift ($C_{L,wing}$)	0.48
Power-off Flap lift increment ($\Delta C_{L,flap}$)	1.8
Lift due to deflected thrust ($C_{L,2}$)	1.16
Lift due to mass flow increase ($C_{L,3}$)	1.1
Estimated Longitudinal force coefficient	
Total Longitudinal force coefficient (C_X)	-0.41
Longitudinal force due to thrust ($C_{X,off}$)	-1.1
Power-off drag ($C_{X,off} = C_{D,i} + C_{D,0}$)	0.32
Power-off induced drag ($C_{D,i}$)	0.25
Power-off, unadjusted profile flap drag ($C_{D,f,p}$)	0.31
Power-off, Adjusted profile flap drag ($C_{D,f,p,A}$)	0.07
Power-on induced drag ($C_{X,3}$)	0.37

Table 4.2.2: Key Example: Flight condition and estimated values at $C'_T = 1.6$ and $\alpha = 0°$, in Wave-off configuration.

4.2.4 Landing configuration

The lift curves, both estimated and experimental, for various thrust coefficients are presented in Fig.4.2.6. The estimated lift values show less than a 10% error compared to the experimental data within the unstalled regime. Experimentally, a maximum lift coefficient of 5.4 is achieved with a thrust coefficient of 1.6.

The longitudinal force and drag polar curves, depicted in Fig.4.2.8, further illustrate the aerodynamic characteristics under landing conditions. As previously discussed, no correction for profile drag was applied due to the extreme flap deflection, which exceeds the maximum estimated deflection. The lift and drag estimations vary from being underestimated to over-

estimated, indicating that the flow associated with this configuration cannot be accurately studied with our simple approach.

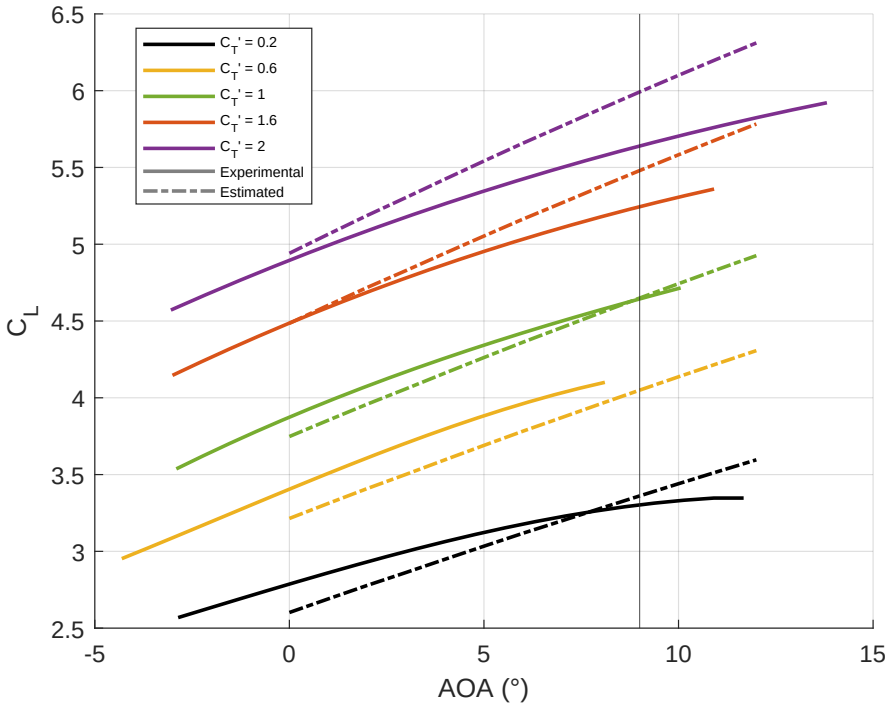

Figure 4.2.6: Lift curve for various thrust coefficient in Landing configuration ($\delta_f = 98/65$) : Estimated vs Experimental values. The horizontal line at $\alpha = 9.5$ represents the end of the unstalled regime computed by ADS.

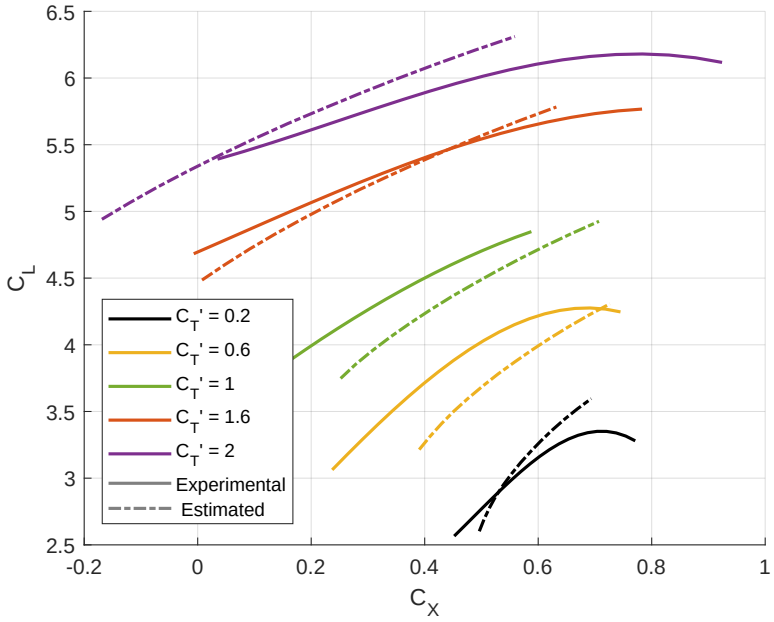

Figure 4.2.7: Longitudinal Force Coefficient Polar.

Figure 4.2.8: Longitudinal Force Polar : Variation with Various Thrust Coefficients (C'_T) in Landing configuration ($\delta_f = 98/65$) : Estimated vs. Experimental values. The experimental values are extracted from [5] and based on flight test data

The estimated values for a specific flight condition (thrust coefficient equal to 1.6 and at zero angle of attack) in the landing configuration are illustrated in Table 4.2.3 , highlighting various key values and parameters. It is shown that, compared to the standard take-off configuration, the lift is increased due to both power-off flap lift increment and slipstream deflection. More than half of the lift is directly attributable to slipstream deflection. However, this increase in lift is achieved with greater thrust deflection, resulting in a worse lift-to-drag ratio.

It is also calculated that the estimated turning angle is higher than the possible turning angle of these flaps, as established by Kuhn. Therefore, the turning angle has been limited to its maximum values.

Configuration Characteristics	Values
Flight Condition	
Total thrust coefficient (C'_T or T'_C)	1.6
Altitude	5000 ft
Weight (W)	37 500 lbs
Center of Gravity position in % of wing chord	30.5%
Flight speed	$\sim$ 53 knots
Angle of attack (α)	0°
Reynolds number based on mean c_w (Re)	$\sim$ 6 040 000
Estimated parameters	
Înboard theoretical Turning angle (θ_1)	50.8°
Înboard Maximum Turning angle ($\theta_{1,MAX}$)	47.5°
Outboard theoretical Turning angle (θ_2)	36.6°
Outboard Maximum Turning angle ($\theta_{2,MAX}$)	35.1°
Thrust recovery factor ($\frac{F}{T}$)	0.91
Estimated Lift coefficient	
Total lift coefficient (C_L)	4.5
Power-off lift ($C_{L,off} = C_{L,wing} + \Delta C_{L,flap}$)	2.48
Power-off Wing lift ($C_{L,wing}$)	0.48
Power-off Flap lift increment ($\Delta C_{L,flap}$)	2
Lift due to deflected thrust ($C_{L,2}$)	1.05
Lift due to mass flow increase ($C_{L,3}$)	0.98
Estimated Longitudinal force coefficient	
Total Longitudinal force coefficient (C_X)	0
Longitudinal force due to thrust ($C_{X,off}$)	-1.05
Power-off drag ($C_{X,off} = C_{D,i} + C_{D,0}$)	0.68
Power-off, profile flap drag ($C_{D,f,p}$)	0.36
Power-on induced drag ($C_{X,3}$)	0.37

Table 4.2.3: Key Example: Flight condition and estimated values at $C'_T = 1.6$ and $\alpha = 0°$, in landing configuration.

4.2.5 Conclusion and Interpretation

The research confirms that lift can be significantly enhanced by deflecting the slipstream, a result that is particularly noteworthy because the increase in lift surpasses what could be achieved with vertically oriented propellers (for a given thrust coefficient). This superiority arises from the increased mass flow within the wing's stream tube, which effectively augments the overall lift generated by the aircraft.

However, the experimental findings highlight a critical trade-off inherent in the blown wing configuration. While substantial lift augmentation is achieved through the deflection of thrust, this comes at the cost of increased drag. Managing this drag is essential to optimizing the overall performance of the aircraft, underscoring the delicate balance that must be maintained in the design and operation of blown wing systems.

The estimation method employed in this study has demonstrated strong accuracy in predicting lift curves but has shown limitations in estimating the drag and particularly, the profile drag of the flaps. To address this issue, a correction factor, which varies with the thrust coefficient, has been introduced. This adjustment improves the estimation of flap profile drag. It is important to note that this correction is only applied within the estimated operational boundaries of the aircraft's configuration.

Overall, the results indicate that when the power-off estimations are accurate, and the flap profile drag is properly adjusted for the blown wing configuration, the estimation method yields reliable results. The analysis of the take-off configuration highlights that accurately estimating power-off characteristics is challenging, as the aerodynamic performance of flaps can vary significantly based on their design. The Breguet's flap design, which shows remarkable performance at high deflection angles, exemplifies the potential for future advancements in flap design to further enhance aircraft performance.

The maximum angle of attack estimated by ADS serves as an approximate indicator of the method's limitations and the onset of flow separation. The maximum flap deflection predicted by Kuhn's method also appears to closely match the experimental maximum flap deflection. Notably, in the landing configuration, which exceeds the estimated maximum turning angle, the large increase in lift, compared to the wave-off configuration, does not occur. Instead, a significant increase in drag is observed, showing that the deflection is too high. This observation is supported by experimental data and aligns with NASA's investigation of the Breguet 941 [5]. The increase in drag in the landing configuration is intentional, and is used to prevent a rise in speed during the approach phase when power is applied.

4.3 X-57

In this section, the lift curve of the X-57, shown in Fig4.3.1, as obtained through extensive CFD simulations conducted by NASA, is briefly compared to the estimated values derived from the rapid estimation method developed in this study. The configuration under investigation is the only one that has been simulated for the takeoff performance of the X-57, featuring flaps deflected at 30 degrees and operating at 58 knots.

The comparison reveals that the estimated lift values align closely with the CFD results within the unstalled regime, although the estimated values tend to be slightly lower. It is important to note that the power-off lift of the wing was found to be overestimated when using the ADS method. This overestimation introduces a greater discrepancy between the predicted and actual blown wing performance, suggesting that the blown wing estimation would likely be less accurate if the power-off lift were correctly assessed.

This comparison also highlights the potential application of the current estimation method, particularly in capturing the, highly distributed, well designed propeller-wing-flaps configuration of the X-57 Maxwell.

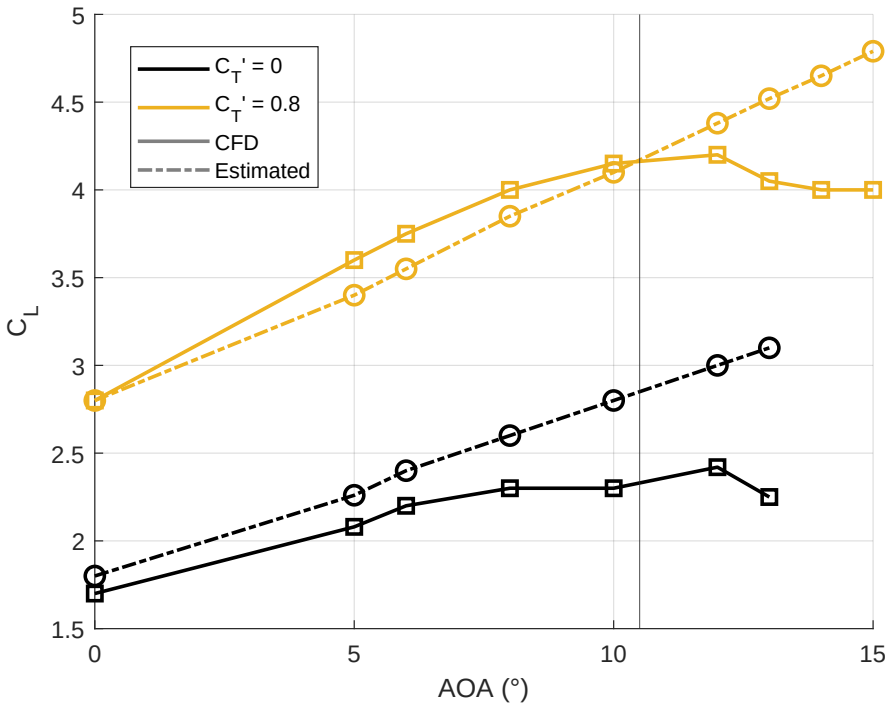

Figure 4.3.1: Lift curve for power-on and off of the X-57 wing ($\delta_f = 30$) : Estimated vs CFD values [23], 58 KTAS, $M = 0.0878$, $Re = 1.33$ million, Altitude= 0,$T = 59°$ and total thrust of 596.4 lbf.

Chapter 5

Performance of Blown wing aircraft

5.1 Regulation and Safety Margin

5.1.1 Introduction

While the regulation related to distributed electric propulsion and blown wings are not the primary focus of this study, this chapter begins by briefly exploring the regulatory limitations and safety margins of these configurations and their impact on performance. Specifically, the conditions for determining stall speed V_S and minimum control speed (V_{MC}) can be significant limiting factors. These speeds are crucial as they determine critical performance parameters such as approach speed for landing, lift-off speed, and overall aircraft safety margins during various phases of flight. Understanding these regulatory constraints is essential for evaluating the viability and performance potential of innovative propulsion and wing configurations.

The discussion will primarily focus on the regulations pertaining to the certification of small aircraft under 14 CFR §23. This regulatory framework has recently been revised and is expected to be the most relevant for new Distributed Electric Propulsion (DEP) blown wing configurations. Notably, some of these regulatory changes specifically address stall speed and approach speed.

Following the regulatory discussion, the effects of ground proximity on wing lift and drag will be examined. General trends will be identified and analyzed based on experimental data and relevant studies. Ultimately, a proposed modification to the drag equation will be introduced to account for the influence of ground effect, aiming to refine the accuracy of performance predictions

Finally, the chapter delves into the performance characteristics of blown wing aircraft. Each performance metric is analyzed in the context of its interaction with the blown wing configuration, using the X-57 and Breguet 941 as case studies. The detailed estimation procedure used to predict these performance metrics is then outlined. Finally, the chapter concludes with a comparison of the estimated performance of the Breguet 941 against experimental data obtained by NASA, highlighting key findings and insights.

5.1.2 Stall Speed regulation

The unique characteristic of blown wing aircraft lies in the coupling of propulsion and lift, meaning that maximum lift is drastically increased with the amount of thrust applied. Previously, under the former regulation , stall speed or minimum speed was defined with the propulsion systems set at idle or zero thrust. This meant that blown wing aircraft would see little to no performance advantage, as their approach speeds (typically $1.3V_stall$) would be constrained by their stall speed in a power-off condition.

However, since a regulatory update in August 2017, stall speed is now defined in 14 CFR § 23.2110 under two conditions:

> (a) Idle or zero thrust for propulsion systems primarily used for thrust, and (b) Nominal thrust for propulsion systems used for thrust, flight control, and/or high-lift systems.

This change in regulation opens the door for distributed propulsion and blown wing configurations, allowing these advanced systems to fully leverage their lift-enhancing characteristics.

The stall speed used for the safety margin during the conceptual design in ADS will therefore be the one calculated according to the method detailed in Chapter **??** under the specific flight conditions to which the speed margin refers. For example, in the case of the landing, the stall speed or minimum speed will be determined with the flap deflection used during this phase and at full power.

Speed margin

With the conditions for establishing stall speed now clear and seemingly in accordance with current regulations, this thesis proposes to adopt the same performance speed margins as those used for conventional aircraft certified with four or more engines. This methodology is likely to be applicable to most blown wing aircraft, given their use of distributed propulsion systems. By maintaining these established speed margins, we can ensure they meet similar safety and performance standards as their conventional counterparts, facilitating their integration into existing regulatory frameworks.

Landing Approach

Regarding the approach speed during landing, there is no longer a reference approach speed defined directly in terms of the stall speed.

The new regulation 14 CFR §23.2130 regarding landing requires:

> (b) The approach and landing speeds, configurations, and procedures, which allow a pilot of average skill to land within the published landing distance

consistently and without causing damage or injury, and which allow for a safe transition to the balked landing conditions of this part accounting for:

1. Stall speed safety margin; and
2. Minimum control speeds.

Regarding this new regulation, a proposal for defining the new safety margin during approach was put forth by Patterson, M. D et al [19]. The key points can be detailed as follows:

1. **Assumption of Lift Coefficient Division:** The proposal assumes that the lift coefficient (C_L) of blown wing aircraft can be divided into two distinct terms. The first term is a function of the angle of attack (α), and the second term is a function of the power setting and thus the blowing effect. This division acknowledges the unique coupling of propulsion and lift in blown wing configurations.

$$C_L = C_{L,\alpha} + C_{L,blowing} \tag{5.1.1}$$

2. **Determination of Conventional Aircraft C_L Margin:** The C_L margin for conventional aircraft, which comply with the former regulation of $V_{\text{approach}} = 1.3V_{\text{min}}$, is established as a benchmark. This C_L margin typically ranges between 0.61 and 0.82. These values provide a reference point for evaluating the safety margins of blown wing aircraft.

3. **Imposition of dual-margin on Blown Wing Aircraft:** The proposal suggests imposing the same C_L margin on the total lift coefficient of blown wing aircraft during approach. This safety margin can be achieved by establishing a margin on the angle of attack, the thrust, or a combination of both. Additionally, a non-zero angle of attack margin is required to ensure sufficient maneuverability and safety under various operational conditions. This dual-margin approach aims to accommodate the unique aerodynamic characteristics of blown wing configurations while maintaining comparable safety standards to conventional aircraft.

While this model offers straightforward rules to follow, it assumes that the power setting and maximum angle of attack are independent variables. This assumption may hold within reasonable bounds for the NX-57 and its high-lift propeller system, but it is not valid for the Breguet 941 or other potential aircraft with higher thrust capacities. As indicated by the lift equation 3.2.15 developed by Kuhn, R.E , the enhanced lift produced by the propeller is function of the angle of attack :

$$C_L = C_{L,off} + \frac{F}{T}C'_T \sin(\theta + \alpha) + k\frac{F}{T}C'_T \sin(\theta + \alpha)\sqrt{\frac{1}{1 + \frac{C'_T S}{N S_p}}} \tag{5.1.2}$$

Moreover, as previously explained and supported by wind tunnel data, the maximum angle of attack is also dependent on the thrust coefficient and, consequently, the power setting.

Additionally, the proposed fixed lift coefficient margin of 0.6 to 0.8 appears insufficient. For example, the Breguet 941 in landing configuration at full power has a stall speed of 44 knots, corresponding to a lift coefficient of 6.7. A safety margin of 0.6 on the lift coefficient equates to a speed margin of approximately 5%, or around 2 knots. This margin is inadequate when considering engine failure and wind-gust conditions. Furthermore, blown wing aircraft are likely to voluntary experience high drag to offset the thrust required for blowing the wing during approach. Hence, a sudden variation in thrust, such as an engine failure or a propeller stopping, could cause a rapid and significant decrease in speed due to this high drag, making a speed margin of 5% seems clearly insufficient in this context.

The proposal put forward by this document is to adopt a safety margin similar to the former regulation concerning stall/minimum speed, determined at full power (nominal power), and also establish an angle of attack margin relative to the power-off maximum angle of attack. This maximum angle of attack is calculated at the (power on) stall speed. Consequently, this maximum AOA is lower than both the maximum AOA with power on and off at any point during the approach. It represents the lower boundary of maximum angle, ensuring a comprehensive safety margin across various operational scenarios.

5.1.3 Minimum control speed

It should be noted that approach speed can also be constrained by maneuverability speed. While this aspect is heavily dependant on the aircraft configuration and will not be detailed or analyzed within the scope of this work, some characteristics pertinent to blown wing aircraft can be highlighted.

1. **Engine Failure Probability and Impact**: Engine failure is more probable due to the number of propellers. However, the impact of an engine failure will be less significant because each engine contributes a lower percentage of the total thrust.
2. **Coupling of Lift and Thrust**: The failure of an engine or propeller induce yawing moment but also a significant rolling moment due to the coupling of lift and thrust. A way to mitigate this issue was used by the Breguet 941 that employs a cross shaft mechanism that distributes the total engine power equally among the four propellers, ensuring balanced thrust and lift distribution.

5.1.4 Further Reading

For more detailed information and discussions, the reader is encouraged to refer to the following articles and dissertation :

Schlickenmaieret, H. W. et al. "X-57 Maxwell Airworthiness Validation Plan"[36]: This document serves as an example certification basis and method of compliance for a distributed electric propulsion airplane under 14 CFR Parts 21, 23, 33, and 35. It outlines the regulatory framework and compliance strategies for the X-57 Maxwell, offering a guide to airworthiness validation in this context.

Patterson, M. D et al. "Approach Considerations in Aircraft with High-Lift Propeller Systems"[19]: This article provides valuable insights into the operational considerations and performance implications of Blown wing systems, particularly in relation to the X-57 and High-Lift Propeller (HLP) configurations. It offers a detailed analysis of approach procedures and their impact on aircraft performance.

Michael D. Patterson's Dissertation: "CONCEPTUAL DESIGN OF HIGH-LIFT PROPELLER SYSTEMS FOR SMALL ELECTRIC AIRCRAFT"[10]. In section 5.1.1 Patterson discusses regulations related to stall and approach speeds. This section provides potential ideas regarding safety margins and new regulations, although it is important to note that the dissertation was written before the latest regulatory updates.

Renselaer,D. J."STOL Tactical Aircraft Investigation, EXTERNALLY BLOWN FLAP."[37]: This document identifies critical STOL safety aspects of externally blown wing configurations for medium-sized transport aircraft with four engines, under the military specification 'MIL-C-5011A.' It includes discussions on safety margins related to engine failure, maneuver capability, and gust response, providing a thorough examination of the safety considerations for STOL operations.

5.2 Influence of Ground Proximity

Estimating the ground effect is a significant challenge in the performance analysis of blown wing aircraft. The impact of ground effect is highly variable, and its magnitude is heavily dependent on the specific configuration of the aircraft. This dependency is influenced by a multitude of interrelated factors, which are difficult to analyze in isolation: wing geometry, the height of the wing and flaps relative to the ground, flap deflection, aircraft speed, thrust coefficient, and more. The ground effect can vary from negligible to substantial and may affect lift, drag, or both, depending on the circumstances.

In this section, we will explore general trends associated with ground proximity, drawing insights from wind tunnel experiments and theoretical models, as detailed in Section 5.2.1. The most reliable and widely used data will be derived from wind tunnel experiments involving externally blown wings by both propeller and turbojet.

The primary model used in this study is derived from the work of Gratzer, L. B., and Mahal, A. S. [38]. Their research proposes that the effects of ground proximity on total lift and drag —excluding the jet momentum generated by the propeller— can be approximated based on the ground effect observed in unblown wings. This hypothesis is supported by experimental results from studies on externally blown flaps powered by turbojet engines. While turboprops produce a higher mass flow and more flow interactions, the study suggests that this methodology could also be applicable to aircraft with propeller-driven systems.

Building on this premise, the analysis of ground effect on blown wings can be segmented into two primary areas: the conventional study of ground effect on wings, which benefits from extensive data and established estimation models, and the analysis of thrust and its deflection in relation to ground proximity.

5.2.1 Case studies

Dans cette subsection,Le resultat de plusieurs key etudes sont detaillés de maniere non exhaustives. D'autres, non précisé ici, seront utilisé comme base pour établir le general trend.

Study 1 : WindTunnel investigation of blown wing near ground

The half-wing investigated is a tapered wing with double slotted deflected at 90°, blown by two propellers in static thrust condition. It is a similar configuration than the Breguet941 during approach.The main characteristics are showed in 5.2.1. As this study is done in static thrust, the focus is only on the force generated by the thrust and therefore the slipstream.

The information and conclusion of this configuration are originated from the study by Kuhn, Richard E :" (en italique) Investigation of the Effects of Ground Proximity and Propeller Position on the Effectiveness of a Wing with Large-Chord Slotted Flaps in Redirecting Propeller Slipstreams Downward for Vertical Take-Off".

Configuration Characteristics	**Values**
Wing	
Area (semispan)	5.125 ft^2
Span (semispan)	3.416 ft
Mean aerodynamic chord	1.514 ft
Root chord	1.75 ft
Tip chord	1.25 ft
Airfoil section	NACA 0015
Aspect ratio	4.55
Taper ratio	0.714
Flap	
Type	Double slotted
Flap chord (in wing chord %)	60%
Deflection	90° Propellers
Diameter (D)	2.0 ft
Nacelle diameter	0.33 ft
Airfoil section	Clark Y
Solidity (each propeller)	0.10

Table 5.2.1: Study 1: Wing and Propeller Characteristics.

Key findings

- The influence of ground effect is initially marked by a reduction in the thrust recovery factor as the ground is approached, followed by a significant loss in turning angle.

- At very low heights above the ground ($h/D = 0.1$), the reduced turning angle leads to an increase in longitudinal force and a decrease in lift compared to conditions at high altitude.
- Visual inspections revealed complete flow separation occurring on the flaps at high deflection.
- When the propeller is positioned at $x/D = 0.25$ and $x/D = 0.42$ relative to the wing, lowering the thrust axis by $0.125D$ below the wing chord plane results in a slight increase in turning angle when the model is outside of the ground-effect region, and a more significant increase when near the ground
- The pitching moment around quarter chord is reduced in ground effect.

Study 2 : Ground Effect in STOL operation

The document titled "Ground Effects in STOL Operation" by L. B. Gratzer and A. S. Mahal of The Boeing Company presents an in-depth analysis of ground effects in Short Takeoff and Landing (STOL) aircraft operations. The study combines theoretical analysis with wind tunnel test data to explore how ground proximity impacts the performance of various STOL configurations.

Key findings

- The methods traditionally used to estimate the ground effect for conventional wings can also be applied effectively to externally blown wings.

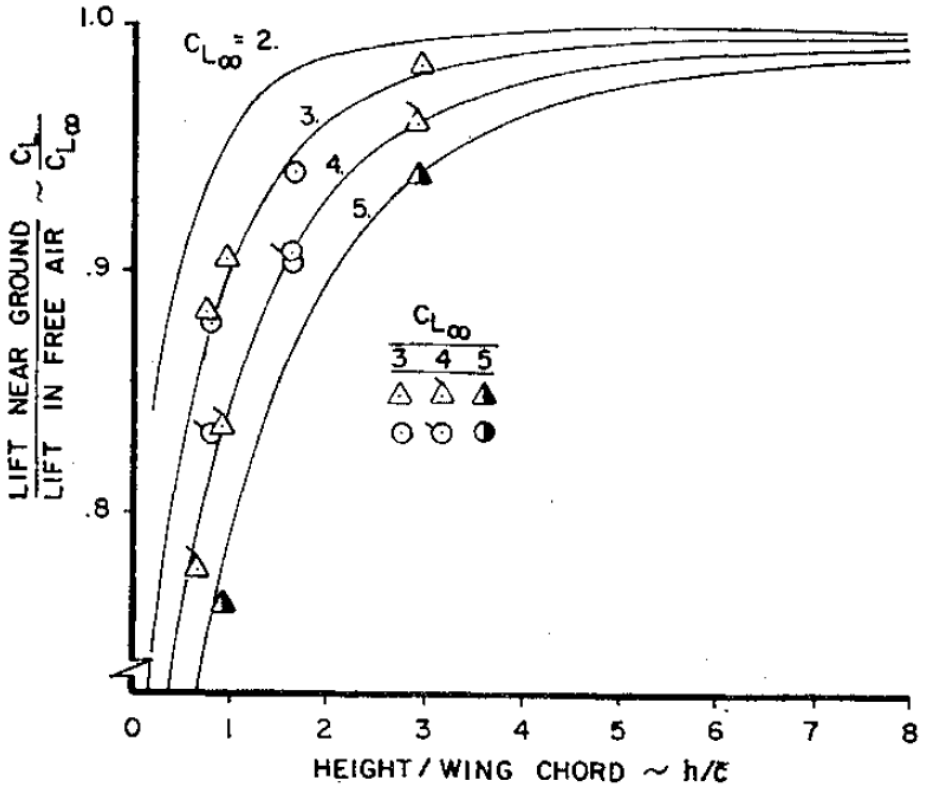

Figure 5.2.1: Lift Ratio In and Out of Ground Proximity vs. Height-to-Wing Chord Ratio: Predictions from the simplified vortex-lattice model compared to experimental data of externally blown flaps. The experimental data were obtained using a turbojet and the influence of jet reaction forces on total lift has been removed from the test data. The graph has been modified and extracted from [38].

- High-wing configurations generally demonstrate superior performance in Ground proximity compared to low-wing configurations for STOL aircraft.
- Ground effect contributes to a noticeable reduction in downwash.
- Swept wings may experience significant changes in pitching moment when flow separation occurs. More, greater attitude is needed to maintain a given lift coefficient (Cl) compared to unswept wings. The authors recommend minimizing wing sweep for STOL operations.
- The impact of ground effect is less significant for high-tail configurations compared to low tails.

Study 3: Unblown Wing in Ground Proximity

This study examines the aerodynamic characteristics of two wing configurations, rectangular and tapered, operating in ground effect, with split and slotted flaps deflected at angles of 40°

and 60°. The range of heights tested spans from 0.5 to 3 h/c_w. The findings are based on the seminal work of Recant, Isidore G., *"Wind-Tunnel Investigation of Ground Effect on Wings with Flaps."*.

Key findings

- The lift slope remains relatively unchanged by ground proximity.
- The maximum lift coefficient decreases across all flap and wing configurations due to an earlier onset of stall.
- The study shows that for all tested heights, the ground effect on wings with flaps is characterized by a significant increase in the lift-to-drag ratio up to the point of maximum lift coefficient, despite the overall reduction in the maximum lift coefficient.
- A noticeable reduction in pitch moment around the quarter chord is observed when the wings are in ground effect.
- Tapered wings demonstrate superior performance in ground proximity compared to rectangular wings.

Conclusion

This section presents several key findings from the analysis of ground effect on blown wings. These principles are intended to serve as guidelines during conceptual design and should not be interpreted as universally applicable for all configurations. Additionally, several of the key findings are based on the assumption that the analysis of blown wings in ground proximity can be segmented into two distinct components: an unpowered wing analysis and a jet momentum analysis. This assumption still requires further validation to ensure its accuracy and applicability across different configurations.

Various studies, not detailed here, have contributed to the establishment of these guidelines. References to these studies are provided at the end of each point and are cited in the bibliography.

- Stall typically occurs at lower angles of attack and with less flap deflection in ground effect compared to conditions outside of it.
- The higher the power-off lift coefficient, the more pronounced the ground effect is, and this effect is observed at greater wing heights.
- High-lift wing-flap configurations do not generally benefit from ground effect in terms of lift slope. [30] [39] [40]
- A noticeable reduction in downwash is observed in the presence of ground effect.[30] [39]
- Ground effect leads to a reduction in pitch moment around the quarter chord.[30] [39]

- Similar to scenarios without propeller slipstream, the general trend for maximum lift coefficient (excluding jet momentum contribution) in ground effect is outlined here. [38]
- Ground effect can have large impact on drag above $\frac{h}{c_w} = 3$ for high lift wing. [40]
- The lift-to-drag ratio can significantly improve before stall, even at flap deflections that drastically reduce maximum lift.[40] [41]
- At high flap deflections (above 50 degrees) and low height, the thrust recovery factor generally decreases, and thrust deflection is also significantly reduced. This results in a higher longitudinal force coefficient and a lower lift coefficient than would otherwise be expected in high altitude.[30] [39]

5.2.2 Estimation procedure

Given the necessity for additional experiments and data to develop a comprehensive procedure for blown wings in ground proximity (and to assess whether such a procedure is feasible), the current estimation approach is constrained to applying corrections on power off induced drag and the $C_{x,3}$ coefficient, as formulated by Wieselsberger and Hoak [42],[43] and emphasized by [44]. This correction is applicable only for flap deflections below 40°.

The change in the power-off induced drag coefficient due to ground effect can be expressed as:

$$\Delta C_{D_i} = -\sigma' \frac{C_L^2}{\pi AR} \tag{5.2.1}$$

With :

- C_L is the lift coefficient in the specific configuration outside of ground effect.
- σ' represents the induced drag correction factor due to ground effect, which can be determined using the following relation:

$$\sigma' = \frac{1 - 1.32(h/b)}{1.05 + 7.4(h/b)}, \quad \text{for } 0.033 < \frac{h}{b} < 0.25 \tag{5.2.2}$$

Here, h/b is the height-to-span ratio.

5.3 Performance Analysis

In the ADS software, performance analysis is handled differently depending on the module in use. In the reverse engineering module, the performance metrics are predefined, and the flight conditions are established accordingly. In contrast, within the performance analysis

module, the flight conditions are provided as inputs, and the resulting performance metrics are calculated. To ensure simplicity and clarity, the performance analysis presented here will utilize the characteristic speeds and flap deflections specific to each flight phase as input. The other parameters, such as power setting and angle of attack, will be estimated to achieve this performance (if possible). The defined parameters are assumed to be either user-specified or derived based on the aircraft's minimum speeds, in accordance with the regulations previously outlined.

If user-defined conditions fail to meet regulatory standards, exceed the stall angle of attack, or surpass the permissible flap deflections, the system will notify the user that the conditions fall outside the range where the applied approximations maintain acceptable accuracy. However, the results can still be displayed.

Adhering to regulations, even with specified flap deflections, still allows for multiple takeoff and landing profiles due to the additional degree of freedom provided by engine-induced lift and the coupling of lift with longitudinal force. Consequently, identifying the optimal performance profile requires an iterative process, which is beyond the scope of this discussion and will not be detailed here.

5.4 Minimum speed

5.4.1 Determination of the Minimum Speed

Traditionally, ADS estimates the stall speed and the corresponding angle of attack using an iterative process. It utilizes aerodynamic airfoil data from XFOIL (for specified Mach and Reynolds numbers and employs), lift increment due to flap and, with other theories, Prandtl's lifting-line theory to calculate the lift distribution across the entire wing. For a given speed, the stall angle of attack is then identified as the angle at which the maximum lift coefficient (Cl_{max}) is exceeded at one of the wing sections. If the lift at this angle is either too high or too low for steady flight, the speed is adjusted iteratively until convergence, where lift equals weight.

For a blown wing, however, the stall angle is influenced by the interaction between the slipstream and the wing. Accurate determination of this interaction typically requires wind tunnel testing or extensive simulations. An alternative method to approximate the actual stall angle involves considering the Reynolds number within the slipstream instead of the freestream. This approach requires further validation and is not currently implemented in ADS.

Consequently, the stall angle of attack for a blown wing will be the one estimated under power-off conditions by ADS. This conservative approach provides a lower limit for the aircraft's performance and ensures safety by preventing immediate stall in the event of multiple engine failures (see section on safety margins).

Therefore, the iterative process for determining the stall speed (or minimum speed for a

blown wing aircraft) remains similar to that of a conventional aircraft, with two key differences: the lift coefficient is estimated using Kuhn's method, and the propeller performance needs to be adjusted each time.

5.4.2 Breguet 941: Minimum speed Estimation vs. Experimental minimum speed

The experimental minimum speeds for the Breguet 941 aircraft, measured in different configurations, are 50 knots for take-off, 46 knots for wave-off, and 44 knots for landing.

Using the ADS approach, the estimated minimum speeds for the same configurations were determined to be 53 knots for take-off, 45 knots for wave-off, and 44 knots for landing. These results indicate a close alignment with the experimental data, particularly for the wave-off and landing configurations. The take-off configuration, however, shows a slight overestimation by 3 knots.

Despite this minor inaccuracy, the results are promising. The ADS approach demonstrates its potential as a viable tool for estimating minimum speeds across various flight configurations. It needs, however, more validation against a broader range of experimental data to ensure its applicability across different aircraft configurations and operational conditions.

5.5 Take-Off

5.5.1 Determination procedure

The forces acting on the aircraft at various points during the ground roll are estimated, and an interpolation is performed between each point. This approach allows for the determination of the aircraft's acceleration at every stage of the ground roll, leading to the calculation of the required distance to reach the lift-off speed. The lift-off itself is initiated by imposing the angle of attack necessary to achieve lift-off at the specified speed. Following this, an iterative process is employed to calculate the climb angle and angle of attacks required to reach the selected speed at 50 feet above ground level. This process is grounded in the analysis of the forces acting on the aircraft at an intermediate speed between the lift-off speed and the speed at 50 feet.

This methodology ensures that all critical aerodynamic and thrust forces are accurately represented throughout the takeoff sequence. The iterative process also accounts for variations in aerodynamic behavior and engine performance.

5.5.2 Breguet 941: Take-Off Estimation vs. Experimental Take-Off

The experimental ground take-off distance and the distance at 50 ft height for the Breguet 941, at a weight of 38,600 lbs, are recorded as 440 ft and 1,000 ft, respectively.

When applying the estimation method developed in this study, the corresponding distances were calculated as 452 ft for the ground roll and 1,114 ft to reach 50 ft height, taking ground effect into account. Without considering ground effect, the estimated distance to 50 ft increases to 1,250 ft.

This comparison indicates that the estimation method provides a reasonably accurate prediction of the take-off distances, particularly when ground effect is considered. The slight discrepancy between the estimated and experimental distances highlights the importance of accounting for ground effect in performance assessments, as it plays a significant role in reducing the required take-off distance. However, the method's sensitivity to the inclusion or exclusion of ground effect also suggests the need for careful consideration of this factor in different operational scenarios.

Overall, the results demonstrate that the estimation approach is capable of producing reliable predictions for the Breguet 941's take-off performance, though the precision of these estimates could be further improved by refining the treatment of ground effect and other contributing factors.

5.6 Landing

5.6.1 General consideration

The landing distance of an aircraft can be divided into two components: the ground roll distance and the air distance. While the ground roll distance can be reduced by factors such as friction and reverse thrust, the most critical parameter remains the touchdown speed, and consequently, the stall speed [45]. The air distance, on the other hand, is influenced by the approach path angle.

Blown wing aircraft are capable of achieving low stall speeds due to their high-lift devices. However, the increased lift generated by these devices also results in higher thrust and, consequently, an increase in longitudinal force. This increase in thrust can be problematic during approach because the aircraft gains gravitational energy rapidly, particularly with a steeper approach angle. To mitigate this additional thrust, several strategies can be employed.

During the conceptual design of the X-57, strategies such as the implementation of air brakes and setting the cruise propellers to windmill mode were considered. Additionally, the small high-lift propellers of the X-57 were designed with a focus on maximizing lift per unit of power, neglecting propeller efficiency and thrust.

In contrast, the Breguet 941 utilizes its four propellers during both cruise and landing

phases, and these propellers are thus designed for high propulsive efficiency. The Breguet employs significant flap deflections of 98°/65° degrees for its triple-slotted inboard and outboard flaps. Compared to its wave-off configuration, which has flap deflections of 75°/50° degrees, this setup does not provide more lift but ensures a substantial increase in drag. This is supported by drag polar data and the document's discussion: *"The stall speeds for the two configurations are nearly the same (43 knots), indicating little difference in the lift characteristics with the two flap deflections, but a significant effect on drag."* These significant deflections are safely utilized due to the design of the Breguet's triple-slotted flaps and the blown configuration, which delays the stall and makes it less abrupt. This allows for very low approach speeds (around 60 knots) while maintaining reliable handling characteristics.

Considering this, several approach profiles are possible due to the coupling of lift and thrust. The various profiles for the Breguet are illustrated in Fig5.6.1.

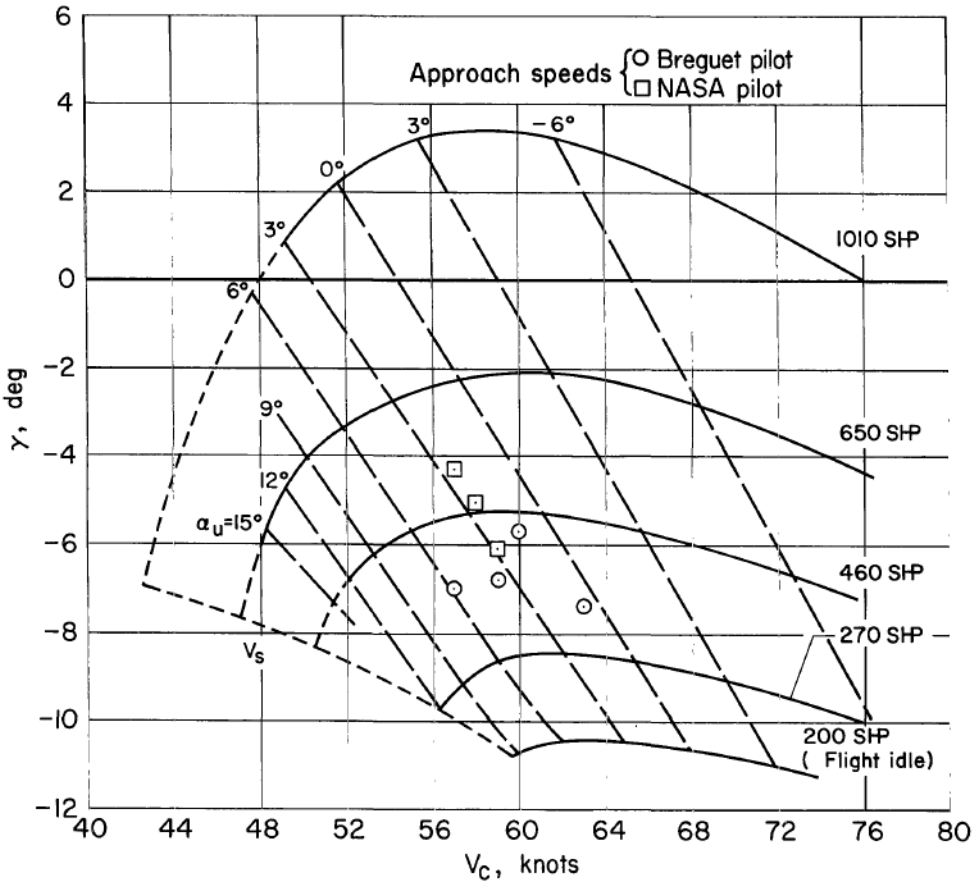

Figure 5.6.1: Landing operational envelope; $\delta_f = 98°/65°$, $W = 38,500$ lb. Extracted from [5]

Generally, increasing the power setting causes higher lift and greater longitudinal force. For the Breguet, this means lower approach speeds can be achieved, but with a shallower approach angle. This results in a shorter ground roll distance but a longer air distance.

Conversely, reducing thrust results in a higher approach speed but a steeper approach angle. This leads to a longer ground roll but a shorter air distance.

The ideal performance parameters depend on the specific aircraft and runway conditions (e.g., grass or asphalt). For the Breguet 941, which is equipped with reverse thrust, Fig5.6.2 clearly shows that it is advantageous to slightly increase the approach speed to achieve a steeper approach angle, even if it results in a slightly longer ground roll.

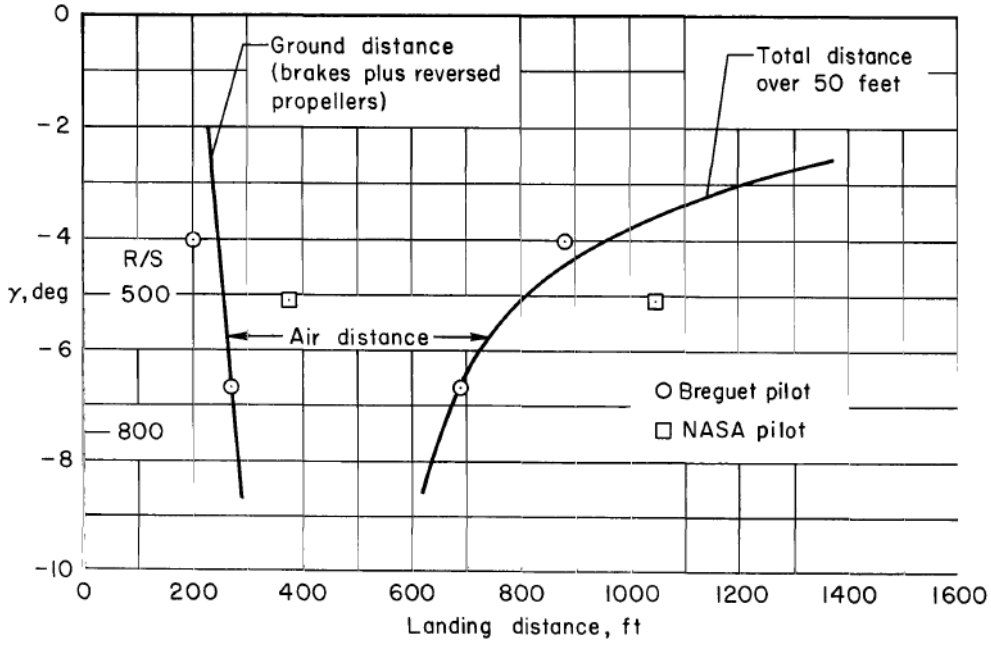

Figure 5.6.2: Variation of landing distance with path angle; $\delta_f = 98°/65°$, $\alpha_i = 3°$, $W = 38,500$ lb. Extracted from [5]

5.6.2 Estimation Methodology

The landing distance is computed by considering three distinct phases: a constant speed approach, a transition phase (half-flare), and the ground roll. The deceleration during the approach is not explicitly modeled and is instead assumed to occur during the transition phase due to an increase in angle of attack, potentially accompanied by a reduction in thrust. This procedure is inspired from the Breguet 941. The short landing procedure for the Breguet 941 involves executing a half flare maneuver to establish the aircraft's attitude for a three-point touchdown with positive sink rate. For more information about approach profile of blown wing aircraft, the reader is advised to read [19] and [5].

The landing distance is then defined as :

$$D_L = D_{GR} + D_{flare} + D_A \tag{5.6.1}$$

With :

- D_{GR}, the ground distance,
- D_{flare}, the half-flare distance

- D_A, the approach distance.

And the distances are computed by :

$$\begin{aligned} D_A &= \frac{h_{screen} - h_{flare}}{\tan(\bar{\gamma_A})} \\ D_{flare} &= R_{flare}\frac{\bar{\gamma}}{2} \\ D_{GR} &= \sum_{n=1}^{b}\left(V_n \Delta t_n + \frac{1}{2}a_n \Delta t_n^2\right) \end{aligned} \tag{5.6.2}$$

With:

- h_{screen} and h_{flare}, the screen height (50 ft for FAR23) and the height at which the half-flare is performed.
- $\bar{\gamma}$, the absolute path angle
- R_{flare}, the radius flare
- a_n, V_n and ΔV_n, acceleration, speed and time intervalls computed at various point of the ground roll distance.

Constant speed approach

For a constant speed approach, the equation of motion are :

$$\begin{aligned} F_x + W\sin\bar{\gamma} = 0 \ (1) \\ L - W\cos\bar{\gamma} = 0 \ (2) \end{aligned} \tag{5.6.3}$$

With W being the weight of the aircraft and :

$$\begin{aligned} F_x &= \frac{1}{2}\rho V_A^2 S_w \times C_x(\alpha, C_T') \\ L &= \frac{1}{2}\rho V_A^2 S_w \times C_L(\alpha, C_T') \end{aligned} \tag{5.6.4}$$

With ρ being the air density and S_w, the surface of the wing

Due to the coupling of lift and thrust, determining the necessary angle of attack (AOA) and power setting (expressed in %) for a specific speed and path angle is not straightforward.

However, by understanding the following principles:

- Increasing power results in higher lift and longitudinal force.
- Increasing AOA results in higher lift but lower longitudinal force.

An iterative process can be utilized. The iterative method implemented in ADS is outlined in the Fig.5.6.3, tailored for a fixed speed and path angle. The maximum angle of attack is set arbitrarily at the stall angle of attack minus 5°. This margin ensures a buffer for safety and allows for an increase in AOA during the transition phase.

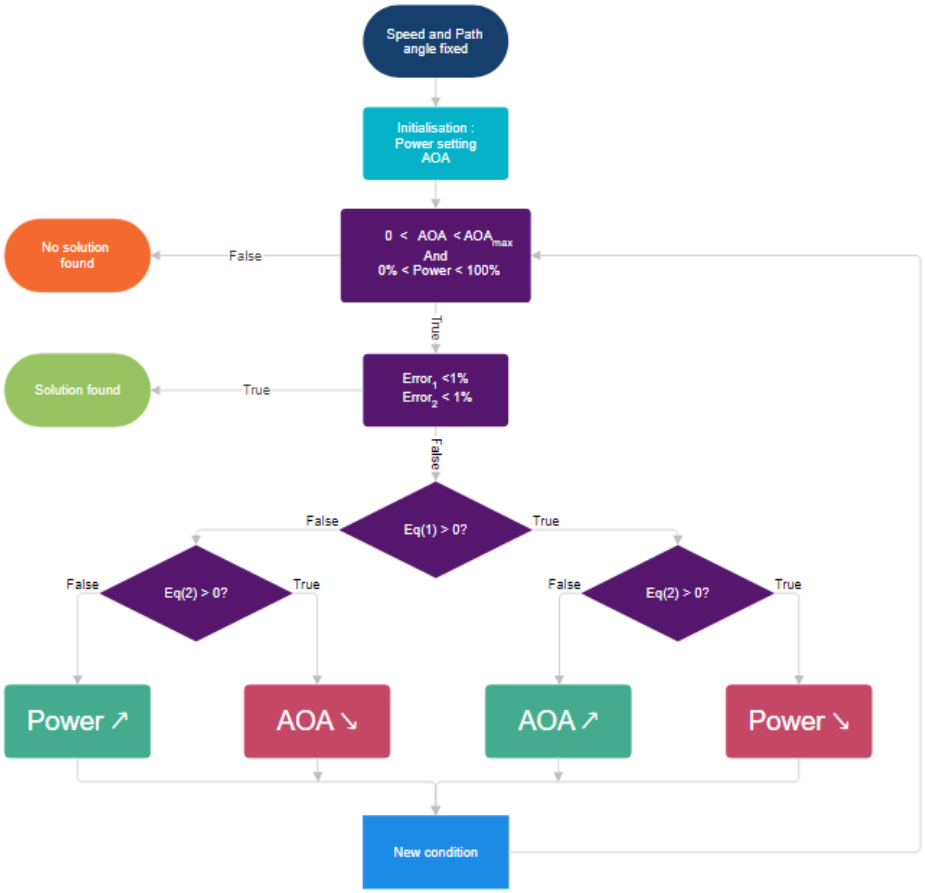

Figure 5.6.3: Flowchart : Iterative process to determine both AOA and power setting for a given speed and path angle during Approach. $Eq(1)$ and $Eq(2)$ are the equations of motion 5.6.3 and $Error_{1,2}$ are defined by 5.6.5

$$\begin{aligned} Error_1 &= \left| \frac{F_x}{W \times \sin \bar{\gamma}} \right| \\ Error_2 &= \left| \frac{L}{W \times \cos \bar{\gamma}} \right| \end{aligned} \tag{5.6.5}$$

Transition

The half-flare path is assumed to be circular, its radius and the height at which it's performed are approximated, with a similar approach than Dr.Roskam [44], by :

$$\begin{aligned} R_{hf} &= \frac{V_A^2}{g(n_{hf}-1)} \\ h_{hf} &= R_{hf}(1-\cos\frac{\bar{\gamma}}{2}) \end{aligned} \tag{5.6.6}$$

With g the gravitational acceleration and n_{HF} the load factor during half-flare.

Ground roll

The ground roll is computed similarly to the take off with the addition of brake and without ground effect.

5.6.3 Breguet 941 : Landing estimation vs experimental data

Accurately estimating the landing performance of the Breguet presents several challenges. Regarding the ground roll, the lack of detailed information on the aircraft's reverse thrust capabilities complicates any precise estimation. Moreover, ground effect is expected to play a significant role during the ground roll, yet there are no established formulas to accurately model this effect. The combined influence of ground effect and reverse thrust further complicates the analysis, rendering it impossible to separate and individually estimate these factors through reverse engineering.

For the approach phase, the flap deflection during landing is so substantial that it exceeds the applicable range of most available estimation formulas. Despite these limitations, two approach scenarios will be analyzed using corrected lift and drag coefficients for the Breguet to assess whether the developed algorithm converges and produces coherent, reliable results.

As illustrated in Table 5.6.1, the estimated power required for both approach scenarios is overestimated. This discrepancy, highlighted in the section related to the Drag polar of the Breguet, arises from the extreme flap deflections, which introduce complex flow dynamics that are challenging to accurately predict. The overestimation of drag and the decrease in thrust recovery factor necessitate a higher power setting to maintain the desired flight path. Moreover, the increased power leads to a reduction in the angle of attack needed, owing to the inherent coupling between power and lift in such configurations.

Landing ($\delta_f = 98°/65°$)	**Parameter**	**Experimental**	**Estimated**
Approach #1	Approach speed, knots	57	57
	Path angle	5°	5°
	Power setting, shp and (%)	520 (47%)	792 (72%)
	Angle of attack	3°	2.1°
Approach #2	Approach speed, knots	61	61
	Path angle	7.5°	7.5°
	Power setting, shp and (%)	330 (30%)	594 (54%)
	Angle of attack	3°	2.4°

Table 5.6.1: Comparison of Experimental and Estimated Approach Performance: Speed and path angle are fixed, with the estimation procedure calculating the required power and angle of attack for a constant speed approach.

Chapter 6

Conclusion

This thesis has provided a comprehensive exploration of the blown wing concept, focusing on the use of propellers and the development of methodologies for performance estimation. A key contribution of this work is the creation of a semi-empirical method, strongly based on Kuhn's approach, and designed for integration into the Aircraft Design Software (ADS) developed by OAD. This method has proven to be a valuable tool, enabling quick and accurate approximations that are particularly useful in the early stages of conceptual design. While the method showed good results for estimating the lift coefficient, it encountered challenges in accurately estimating the longitudinal force.

In exploring the underlying physics of the blown wing phenomenon, particular emphasis was placed on Kuhn's semi-empirical approach. This method leverages momentum theory to estimate aerodynamic forces by incorporating both the classical lift and drag coefficients of a conventional wing and the additional forces induced by the deflection of the propeller slipstream. While this approach remains an approximation, it enables a more nuanced understanding of the aerodynamic characteristics inherent to blown wing configurations.

Kuhn's method was meticulously integrated into the Aircraft Design Software (ADS), in conjunction with supplementary estimation techniques, such as those detailed in Roskam. These methods were predominantly utilized to estimate the lift and drag increments associated with flap deflection. However, it was revealed that this aspect of the methodology poses a significant limitation, as variations in flap design and thrust coefficient can substantially affect the aerodynamic performance of the wing. Moreover, the developed method is confined to application within the unstalled regime of the blown wing—a regime that is challenging to delineate due to the propeller slipstream's ability to significantly delay stall onset. Nonetheless, by employing classical Prandtl line theory and empirical estimates derived from Kuhn's approach, the maximum angle of attack and flap deflection were estimated. Although this method remains an approximation, it demonstrated satisfactory results, aligning closely with experimental data in predicting the onset of flow separation and stall.

The thesis also examined the lift and drag characteristics of blown wing aircraft, using both experimental data and the results of 3D wind tunnel experiments replicated in ADS. The comparative analysis demonstrated that the developed estimation method provides robust predictions, particularly in the lift coefficient, although challenges remain in accurately

estimating the longitudinal force. Additionally, the analysis of the Breguet 941 and X-57 Maxwell, derived from both flight data and CFD simulations. The investigation of the X-57 and the Breguet, which are radically different in terms of propulsion architecture and wing design, have demonstrated the broad applicability of the method.

Finally, the operational performance of blown wing aircraft was explored, with particular focus on takeoff, landing, and minimum speed. The comparison between Breguet's flight data and the developed estimation methods provided further validation of the methodology, confirming its effectiveness in conceptual design phases.

To conclude, this work paves the way for several promising avenues of future research. One key area for further investigation is the accurate estimation of flap efficiency and profile drag in the context of blown wing configurations. Understanding and modeling these aerodynamic characteristics are crucial for improving performance predictions and optimizing the design of such systems. Additionally, developing methods to estimate the impact of ground effect on blown wing performance presents a significant challenge. Ground effect can either enhance or severely limit the performance of blown wings, but creating a reliable predictive method may prove to be complex and possibly unattainable with current knowledge.

Furthermore, although initial steps were taken during the internship at OAD, there is a compelling need to develop an iterative design process specifically tailored for blown wing aircraft. This process would focus on key parameters such as the propulsion system, flap size, and type, aligning these elements with specific performance requirements. Developing such a methodology would require extensive research and a considerable time investment, making it a worthwhile but ambitious goal for future work beyond the scope of this thesis.

Bibliography

[1] M. D. Moore and B. Fredericks. Misconceptions of electric propulsion aircraft and their emergent aviation markets. Technical report, NASA Langley Research Center, Hampton, Virginia, 2014.

[2] C. B. Courtin, A. Mahseredjian, A. J. Dewald, M. Drela, and R. J. Hansman. A performance comparison of estol and evtol aircraft. Technical Report ICAT-2021-02, MIT International Center for Air Transportation (ICAT), Department of Aeronautics & Astronautics, Massachusetts Institute of Technology, Cambridge, MA, USA, 2021.

[3] R. E. Kuhn. Semiempirical procedure for estimating lift and drag characteristics of propeller-wing-flap configurations for vertical- and short-take-off-and-landing airplanes. (NASA MEMO 1-16-59L), 1959.

[4] D. Reckzeh. Aerodynamic design of the a400m high-lift system. In *26th International Congress of the Aeronautical Sciences (ICAS)*, Bremen, Germany, 2008. ICAS, Airbus, Aerodynamics Domain.

[5] H. C. Quigley, R. C. Innis, and C. A. Ho Zzhuuser. A flight investigation of the performance, handling qualities, and operational characteristics of a deflected slipstream stol transport airplane having four interconnected propellers. *Ames Research Center*, 1969.

[6] J. K. Viken, S. A. Viken, K. A. Deere, and M. B. Carter. Design of the cruise and flap airfoil for the x-57 maxwell distributed electric propulsion aircraft. In *AIAA Aviation Forum*, Denver, CO, 2017. NASA Langley Research Center.

[7] B. L. Litherland, N. K. Borer, and N. S. Zawodny. X-57 "maxwell" high-lift propeller testing and model development. *AIAA Aviation Forum*, 2021.

[8] K. A. Deere, J. K. Viken, S. A. Viken, M. B. Carter, M. R. Wiese, and N. L. Farr. Computational analysis of the x-57 maxwell airplane at unpowered conditions (preliminary fuselage). Technical Report NASA/TM-20210011034, NASA Langley Research Center, Hampton, Virginia, 2021.

[9] P. Jackson, editor. *Jane's All the World's Aircraft 2007-2008*. Jane's Information Group, Coulsdon, Surrey, UK, 2007. ISBN 9780710627926.

[10] M. D Patterson. *Conceptual Design of High-Lift Propeller Systems for Small Electric Aircraft*. PhD thesis, Georgia Institute of Technology, 2016.

[11] . Veldhuis. *Propeller Wing Aerodynamic Interference*. Phd dissertation, Delft University of Technology, Delft, Netherlands, June 2005.

[12] M. H. Roe and D. J. Renselaer. Stol tactical aircraft investigation, externally blown flap. volume ii. design compendium. Technical report, Rockwell International Corporation, 1973.

[13] S. J. Miley, R. M. Howard, and B. J. Holmes. Wing laminar boundary layer in the presence of a propeller slipstream. *Journal of Aircraft*, 25(7):606–611, 1988.

[14] R. M. Howard, S. J. Milley, and B. J. Holmes. An investigation of the propeller slipstream on a laminar wing boundary layer. In *SAE Paper No. 850859*, 1985.

[15] F. M. Catalano. On the effects of an installed propeller slipstream on wing aerodynamic characteristics. *Acta Polytechnica*, 44(3):1–10, 2004.

[16] H. Aminaei, M. D. Manshadi, and A. R. Mostofizadeh. Experimental investigation of propeller slipstream effects on the wing aerodynamics and boundary layer treatment at low reynolds number. *Proceedings of the Institution of Mechanical Engineers, Part G: Journal of Aerospace Engineering*, 232(9):1691–1703, 2018. doi: 10.1177/0954410018791703.

[17] H. Aminaei, A. R. Mostofizadeh, and M. D. Manshadi. Experimental and numerical study of wing boundary layer behavior in propeller flowfield. *Journal of Visualization*, 22(2):329–341, 2019. doi: 10.1007/s12650-019-00553-w.

[18] M.D. Patterson, J.M. Derlaga, and N.K. Borer. High-lift propeller system configuration selection for nasa's sceptor distributed electric propulsion flight demonstrator. 2016.

[19] M.D Patterson and N. K. Borer. Approach considerations in aircraft with high-lift propeller systems. Technical report, NASA Langley Research Center, Hampton, VA, USA, 2017.

[20] A. M. Stoll. Comparison of cfd and experimental results of the leaptech distributed electric propulsion blown wing. In *15th AIAA Aviation Technology, Integration, and Operations Conference*, number AIAA 2015-3188, Dallas, TX, June 22-26 2015. AIAA. doi: 10.2514/6.2015-3188.

[21] J. Roskam. *Airplane Design*. Number pt. 6 in Airplane Design. DARcorporation, 1985. ISBN 9781884885525.

[22] R. E. Kuhn. Investigation at zero forward speed of a leading-edge slat as a longitudinal control device for vertically rising airplanes that utilize the redirected-slipstream principle. Technical Report Technical Note 3692, National Advisory Committee for Aeronautics (NACA), Langley Aeronautical Laboratory, Langley Field, Va., 1956.

[23] K. A. Deere, J. K. Viken, S. A. Viken, M. B. Carter, M. R. Wiese, and N. Farr. Computational analysis of a wing designed for the x-57 distributed electric propulsion aircraft. In *AIAA Aviation Forum*, Denver, CO, 2017. NASA Langley Research Center.

[24] M. Nitz and D. Scholz. Estimating the oswald factor from basic aircraft geometrical parameters. In *Deutscher Luft- und Raumfahrtkongress 2012*, Hamburg, Germany, 2012. Hamburg University of Applied Sciences, Aero – Aircraft Design and Systems Group.

[25] D. R. Agrawal, F. As'ad, B. Berk, T.r Long, J. Lubin, C. Courtin, J. Thomas, R. J. Hansman, and M. Drela. Wind tunnel testing of a blown flap wing. *Massachusetts Institute of Technology*, 2015.

[26] G. N. Hawkswell, R. J. Miller, and G. Pullan. Selection of propeller-wing configuration on blown wing aircraft. *Whittle Laboratory, Department of Engineering, University of Cambridge*, 2003.

[27] R. R. Duivenvoorden, N. Suard, T. Sinninge, and L. L. M. Veldhuis. Experimental investigation of aerodynamic interactions of a wing with deployed fowler flap under influence of a propeller slipstream. In *AIAA AVIATION 2022 Forum*, Chicago, IL & Virtual, 2022. American Institute of Aeronautics and Astronautics (AIAA). doi: 10.2514/6.2022-3216.

[28] M. Burston, K. Ranasinghe, A. Gardi, V. Parezanović, R. Ajaj, and R. Sabatini. Design principles and digital control of advanced distributed propulsion systems. *Energy*, 241: 122788, 2022. doi: 10.1016/j.energy.2021.122788.

[29] C. J. Wenzinger. Pressure distribution over an airfoil section with a flap and tab. Technical Report Report No. 574, National Advisory Committee for Aeronautics (NACA), 1936.

[30] R. E. Kuhn and Jr. Hayes, W. C. Wind-tunnel investigation of longitudinal aerodynamic characteristics of three propeller-driven vtol configurations in the transition speed range, including effects of ground proximity. Technical Report Technical Note D-55, National Aeronautics and Space Administration (NASA), Langley Research Center, Langley Field, Va., 1960.

[31] R. E. Kuhn and J. W. Draper. Investigation of effectiveness of large-chord slotted flaps in deflecting propeller slipstreams downward for vertical take-off and low-speed flight. Technical Report Technical Note 3364, National Advisory Committee for Aeronautics (NACA), Langley Aeronautical Laboratory, Langley Field, Va., 1955.

[32] E. Obert. A method for the determination of the effect of propeller slipstream on static longitudinal stability and control of multi-engined aircraft. Technical report, Report LR-761, December 1994.

[33] T. Bouquet and R. Vos. Modeling the propeller slipstream effect on lift and pitching moment. In *AIAA SciTech Forum, 56th AIAA Aerospace Sciences Meeting*, Grapevine, TX, 2017. Delft University of Technology.

[34] R. D. Finck and D. E. Hoak. *USAF Stability and Control Datcom: Revised Edition.* Flight Control Division, Air Force Flight Dynamics Laboratory, Wright-Patterson Air Force Base, Dayton, Ohio, 1978.

[35] R. E. Kuhn and Jr. Hayes, W. C. Wind-tunnel investigation of longitudinal aerodynamic characteristics of three propeller-driven vtol configuration in the transition speed range, including effecs of ground proximity. 1960.

[36] H. W. Schlickenmaier, M. Anderson, E. Harrison, E. H. Hooper, J. Knickerbocker, M. Larson, J. Lawson, M. Voss, R. Wilkinson, and J Turnberg. X-57 maxwell airworthiness validation plan. Technical Report NASA/CR-20220015049, NASA Langley Research Center, Hampton, VA, USA, February 2023.

[37] M. H. Roe and D. J. Renselaer. Stol tactical aircraft investigation, externally blown flap. volume iii. performance methods and takeoff and landing rules. Technical report, Rockwell International Corporation, 1973.

[38] L. B. Gratzer and A. S. Mahal. Ground effects in stol operation. *Journal of Aircraft*, 9 (3):236–243, 1969. doi: 10.2514/3.58963.

[39] R. E. Kuhn. Investigation of the effects of ground proximity and propeller position on the effectiveness of a wing with large-chord slotted flaps in redirecting propeller slipstreams downward for vertical take-off. Technical Report Technical Note 3629, National Advisory Committee for Aeronautics (NACA), Langley Aeronautical Laboratory, Langley Field, Va., March 1956. Technical Report.

[40] I. G. Recant. Wind-tunnel investigation of ground effect on wings with flaps. Technical Report Technical Note 705, National Advisory Committee for Aeronautics (NACA), Langley Memorial Aeronautical Laboratory, Washington, D.C., May 1939. Technical Report.

[41] V. Tremblay Dionne and T. Lee. Ground effect on the aerodynamics of a naca 0015 airfoil with a plain trailing-edge flap. *Fluid Mechanics Research International Journal*, 2(1):1–12, 2018. doi: 10.15406/fmrij.2018.02.00025.

[42] C. Wieselsberger. Wing resistance near the ground. Technical Report Technical Memorandum 77, National Advisory Committee for Aeronautics (NACA), 1922.

[43] D. E. Hoak. Usaf stability and control datcom. Technical report, Air Force Flight Dynamics Laboratory, Wright-Patterson Air Force Base, Ohio, April 1978.

[44] J. Roskam and Ch. T. E. Lan. *Airplane Aerodynamics and Performance*. DARcorporation, Lawrence, Kansas, USA, 1997.

[45] F. May and C. A. Widdison. Stol high-lift design study: Volume i. state-of-the-art review of stol aerodynamic technology. Technical Report AFFDL-TR-71-26-VOL I, The Boeing Company, Air Force Flight Dynamics Laboratory (AFFDL), Wright-Patterson AFB, Ohio, April 1971.